Title

Electronic structure calculations permit identification of the driving forces behind frequency shifts in transition metal monocarbonyls

Journal

Physical Chemistry Chemical Physics, 22(2)

ISSN

0956-5000

Authors

Rossomme, Elliot
Lininger, Christianna N
Bell, Alexis T
et al.

Publication Date

2020-01-02

DOI

10.1039/c9cp04643g

Peer reviewed

Journal Name

ARTICLE TYPE

Cite this: DOI: 00.0000/xxxxxxxxxx

Electronic structure calculations permit identification of the driving forces behind frequency shifts in transition metal monocarbonyls†

Elliot Rossomme[a], Christianna N. Lininger[b,c], Alexis T. Bell[b,c], Teresa Head-Gordon[a,b,c,d], and Martin Head-Gordon*[a,b]

Received Date
Accepted Date

DOI: 00.0000/xxxxxxxxxx

We report the adiabatic energy decomposition analysis (EDA) of density functional theory (DFT) results, shedding light on the physical content of binding energies and carbon monoxide (CO) frequency (υ_{CO}) shifts in select first-row transition metal monocarbonyls (MCOs; M = Ti^-, V^-, Cr^-, Co^-, Ni^-, Cu^-, V, Cr, Mn, Ni, Cu, Zn, Cr^+, Mn^+, Fe^+, Cu^+, and Zn^+). This approach allows for the direct decomposition of υ_{CO}, in contrast to previous studies of these systems. Neutral, anionic, and cationic systems are compared, and our results indicate that the relative importance of electrostatic interactions, intramolecular orbital polarization, and charge transfer can vary significantly with the charge and electron configuration of the metal participating in binding. Various anomalous systems are also discussed and incorporated into a general model of MCO binding. Electrostatic interactions and orbital polarization are found to promote blue shifts in υ_{CO}, while charge transfer effects encourage υ_{CO} red-shifting; experimentally observed values of υ_{CO} are found to be a result of a complex but quantifiable interplay between these physical components. Our computations indicate that $CuCO^-$ and ZnCO possess triplet ground states, and also that $CrCO^-$ exhibits a non-linear geometry, all in contrast to previous computational results. Advantages and limitations of this model as an approximation to more complicated systems, like those implicated in heterogeneous catalysis, are discussed. We also report benchmark results for MCO geometries, binding energies, and harmonic CO frequencies, and discuss the validity of single-reference wave function and DFT approaches to the study of these transition metal systems.

1 Introduction

Transition metal carbonyls possess historical and contemporary interest across a broad range of chemical disciplines. These compounds served as an early and paradigmatic example of synergistic charge transfer interactions in transition metal complexes, and their study elucidates many of the general features of transition metal chemistry.[1] Furthermore, the interaction between transition metals and carbon monoxide (CO) is a critical feature of interactions in catalytic systems.[2–4] Transition metal chemistry is also regarded as a final frontier in modern electronic structure theory. Computationally tractable methods can now yield reasonable predictions for select transition metal systems, though many difficulties remain.[5–10] Hence, theoretical study of metal carbonyls serves as a test for state of the art of computational chemistry. Though among the simplest transition-metal systems, controversy has surrounded the electronic structure of bonding in metal carbonyls, and a variety of models have been proposed to explain the properties of these compounds.

1.1 The Dewar–Chatt–Duncanson Model

The Dewar–Chatt–Duncanson (DCD) model,[11,12] originally proposed for metal-olefin systems, is frequently invoked to explain aspects of bonding in molecular metal carbonyls.[13–38] Within this model, two types of orbital interactions give rise to the bond between the metal atom (M) and CO: (1) electron donation from the slightly antibonding CO 5σ-orbital into unoccupied M orbitals of appropriate symmetry (Figure 1a) and (2) electron donation from occupied M orbitals into the unoccupied 2π^*-orbital on CO (Figure 1b). These interactions are variously referred to as forward- and back-donation or σ- and π-donation, respectively;

[a] Kenneth S. Pitzer Center for Theoretical Chemistry, Department of Chemistry, University of California, Berkeley, California 94720, USA
[b] Chemical Sciences Division, Lawrence Berkeley National Laboratory, Berkeley, California 94720, USA
[c] Department of Chemical and Biomolecular Engineering, University of California, Berkeley, California 94720, USA
[d] Department of Bioengineering, University of California, Berkeley, California 94720, USA
*Fax: +1(510)643-1255; Tel: +1(510)642-5957; E-mail: mhg@cchem.berkeley.edu

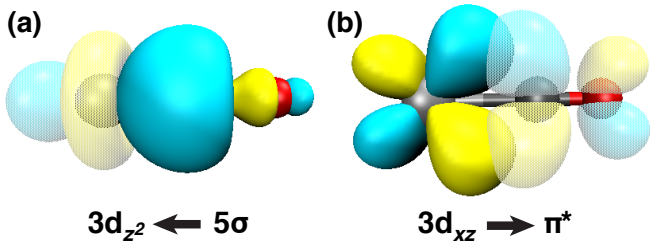

Fig. 1 Dominant orbital interactions in the Dewar–Chatt–Duncanson model of metal-carbonyl binding: (a) forward donation from the CO σ orbital into unoccupied metal orbitals of appropriate symmetry (in this case $3d_{z^2}$); (b) back donation from occupied metal d orbitals (here, $3d_{xz}$) into the unoccupied CO π^* orbital. Orbitals pictured here obtained using COVP analysis on VCO^-.

we use these terms interchangeably throughout. While both modes of donation are understood to stabilize the MCO complex energetically, they are thought to give rise to competing effects in the properties of the CO adsorbate: the loss of electron density from the (slightly antibonding) 5σ-orbital strengthens the CO bond, decreasing its bond length (r_{CO}) and increasing its vibrational frequency (υ_{CO}), while donation into the $2\pi^*$-orbital weakens this bond, leading to an increase in r_{CO} and a decrease in υ_{CO}. Hence, the DCD model provides a possible, charge-transfer-based explanation for differences in observed CO vibrational frequencies across metal carbonyls in terms of the relative importance of forward- and back-donation in a particular system.

Despite its continued popularity, shortcomings of the DCD model have been well-documented, particularly as it concerns the properties of the C−O bond in the complex, which are evidenced by υ_{CO}. While the DCD model has enjoyed success describing trends in metal carbonyls with red-shifted values of υ_{CO} upon binding,[14,22,24,28] its use in explaining υ_{CO} blue shifts is questionable. Explanations in terms of donation from the slightly antibonding 5σ-orbital once seemed plausible,[24,39] but subsequent computational studies indicated that electrostatic and polarization effects drive υ_{CO} blue shifts in metal carbonyls, if they are present.[25,40] As it concerns the complex binding energy (ΔE_{bind}), various studies have indicated that electrostatics, orbital polarization, forward-donation, and back-donation can all play determining roles depending on the system.[15,22,24] Recent experimental accounts of transition metal carbonyls draw on this body of literature to make qualitative explanations of binding phenomena based on both electrostatic effects and orbital interactions.[33–35]

1.2 Alternative Pictures of M−CO Bonds

More detailed quantification of these physical effects in various systems aids in understanding the nature of the metal–carbonyl bond in more complicated and experimentally relevant systems. Previous approaches to this problem can be divided into two broad categories. Some have analyzed computed bond orders and charge migration to evaluate the roles of forward- and back-donation in complexes,[13,23–25,32,39–45] while others track complex binding energies to evaluate the importance of various physical components to the overall M−CO bond.[15,21,27,43,46–49] These two approaches have led to a variety of different conclusions regarding the forces that bind metal carbonyls.

Studies into charge and bond migration in metal carbonyls have typically focused on determining the relative importance of σ- and π-donation in stabilizing metal carbonyls, though no consensus has been reached. Most of this controversy has surrounded the question of whether and to what extent σ-donation contributes to the bond energies and C−O bond properties in metal carbonyls. Early computational studies on select species have indicated that σ-donation is essential to bond formation,[13,39,41,42] while others suggest it is essentially non-existent.[32,40] Comparative studies across a number of species have been particularly illumining in this respect. The charge decomposition analysis (CDA) studies of Frenking *et al.*[23–25] indicated σ-donation is always more significant than π-donation for stabilization of the M−CO bond, and that the relative importance of π-donation decreases from anionic to neutral to cationic systems. They also emphasized the importance of orbital polarization in stabilizing metal carbonyls regardless of charge,[24] and for effecting blue shifts in υ_{CO} for cationic systems.[25]. On the basis of their Mulliken population analyses, Barnes, Bauschlicher, and coworkers have also argued that π-donation plays a minimal role in cationic metal carbonyls, where electrostatic and polarization effects tend to dominate the interaction.[44,45] Others have put forward similar arguments.[32]

The description of metal–carbonyl bonding that has emerged from energy decomposition analysis (EDA), constrained space orbital variation (CSOV),[46] as well as other approaches for analysis of M−CO binding energies is somewhat different. All of these methods proceed by running constrained computations on metal carbonyls and analyzing the changes in ΔE_{bind} as various constraints are removed. CSOV studies of a variety of metal carbonyls by Bagus, Bauschlicher, *et al.*[15,43,46] indicated that π-donation and metal orbital polarization each contributed to binding energies more significantly than σ-donation in most cases, though they found σ- and π-donation to be on the same order in $Fe(CO)_6$.[47] Other results have indicated that σ-electrons contribute the lion's share of the bonding energy between an Fe cluster and CO.[21] Similarly, a series of Morokuma EDA[50,51] studies of $Cr(CO)_6$ indicated electrostatics drive bonding through penetration of CO 5σ-electrons into the Cr valence space, though orbital polarization and π-donation were also found to be important.[48,49] Another EDA study found that complex charge (paradoxically) promotes bond covalency, that σ-donation dominates cations, and that the importance of π-donation increases as a species becomes more anionic.[27] This is in contrast with previous results that suggested certain cationic metal carbonyls are bound by electrostatics.[19,45,52,53]

While the preceding literature survey has focused on molecular metal carbonyls, a brief discussion of current models of the interaction between extended metal systems and CO helps to situate this work within a broader context. Much as the DCD model serves as a paradigm for molecular metal carbonyls, the Blyholder model[54,55] provides the basis for understanding the metal-carbonyl interaction in extended systems. This model is similar to the DCD model in content, explaining the M−CO bond

in terms of charge transfer, although only π-donation was considered in its original formulations. Subsequent studies have expanded upon and refined the Blyholder model, indicating that orbital polarization, σ-donation, and π-donation all seem to play important roles in the formation of M−CO bonds and shifts in υ_{CO}.[4,56,57] Suffice it to say, similar interactions promote the formation of M−CO bonds whether the metal in question is a single atom or an extended surface; in both system classes, the relative importance of these interactions is contested.

Taken together, the extant computational literature indicates that electrostatics, orbital polarization, σ-donation, and π-donation can all contribute significantly to binding in metal carbonyls, although the interplay between these features is subtle, depending on the system of interest and the computational methods employed. Most of this literature focuses on understanding contributions to electronic binding energies of these complexes. Still, the properties of the C−O bond are frequently discussed as well, and these are typically inferred on the basis of the ΔE_{bind} decomposition. If a given component of the physics is the major contribution to ΔE_{bind}, it is assumed to also drive shifts in υ_{CO}. Such an analysis is problematic because C−O bond properties do not correlate well with ΔE_{bind}. In particular the magnitude of υ_{CO} has been shown to vary independently of that of ΔE_{bind}.[24,58,59] Only a few direct investigations into the sources of C−O properties in metal carbonyls have been completed.[25,40,60] The two most noteworthy of these focused on cationic systems, indicating that electrostatic and polarization effects, rather than σ-donation as suggested by the DCD model, drive blue shifts in υ_{CO}.[25,40] Beyond these, a comprehensive and direct investigation into the properties of the C−O bond in metal carbonyls is absent from the literature.

1.3 Scope of the Current Study

Our primary purpose is to provide a coherent model of υ_{CO} shifts in molecular metal carbonyls. This is a vast topic, and we choose to limit the scope of our investigation to metal monocarbonyls (MCOs). Relative to polycarbonyls, which have also been the subject of much research, MCOs carry two major advantages for our purposes: (1) these systems better approximate the metal surface–CO interaction relevant to heterogeneous catalysis[2,15,46,54] and (2) the smaller size of MCOs admits the use of more sophisticated electronic structure methods.

Still, even limited to three-atom MCO systems, computational modeling of transition metal chemistry proves formidable with density functional theory (DFT).[6] It was therefore important to select MCO systems expected to possess relatively straightforward electronic structure. Furthermore, because the effects of overall charge bear significantly on vibrational frequency shifts in these systems,[28] we consider isoelectronic series of anionic, neutral, and cationic complexes. With these two concerns in mind we have modeled the MCO complexes of all first-row atoms and ions that are expected to have a low-lying configuration with either a half- or completely-filled 3*d*-shell. This includes the neutral complexes of V, Cr, Mn, Ni, Cu, and Zn, as well as the singly ionized systems that are isoelectronic to them. We did not consider $GaCO^+$ even though it is isoelectronic with $CuCO^-$ and ZnCO, as Ga is not a transition metal.

We analyze the properties of the C−O bond in these systems using the adiabatic EDA approach of Head-Gordon and coworkers,[38,61] discussed in more detail in Section 2.2 below. This EDA scheme differs from the Morokuma[50,51] and CSOV[46] methods discussed above in that it is fully variational, allowing for geometry optimizations and harmonic vibrational frequency computations at each stage in the decomposition. As demonstrated by Bagus and Pacchioni for CO adsorbed to Au clusters, the CSOV method can be used to decompose $\Delta\upsilon_{CO}$ directly,[60] though most previous uses of EDA schemes, including CSOV, did not analyze the properties of CO in these complexes.[15,21,27,43,46–48,52] In the case of Ref. 60, υ_{CO} was analyzed by fixing the M−CO distance before constructing potential energy curves as a function of r_{CO} that could be used to approximate υ_{CO}, leading to discrepancies between their decomposition analysis and the frequency shift they determined through unconstrained computations. In contrast to these methods, we are able to determine normal modes for MCOs through diagonalization of the Hessian matrix at each stage in our decomposition. This leads to a more physically meaningful and direct analysis of $\Delta\upsilon_{CO}$ in the systems of interest.

The remainder of this manuscript is organized as follows. In Section 2 we describe in more detail our computational procedures and EDA scheme. We then provide validation for our DFT treatment of the systems of interest through comparison to coupled-cluster computations and experimental results (Section 3.1). Having demonstrated the fidelity of our DFT results for these systems, we report EDA results that provide a general model for the physical content of binding energies and frequency shifts in MCO cations, anions, and neutrals in Section 3.2. Finally, we consider some anomalous results (Section 3.3) and conclude with a presentation of a general model for carbonyl binding that includes these outlying systems.

2 Computational Methods

The metal carbonyl (MCO) species of interest were computationally studied using both correlated wave function and density functional theory (DFT) approaches. Geometric parameters and harmonic vibrational frequencies were evaluated using the def2-TZVPD basis set,[62,63] while the larger def2-QZVPD basis[63,64] was employed for single-point energy (SPE) computations at the def2-TZVPD geometries. Harmonic vibrational frequencies were determined through diagonalization of the full Hessian matrix, and optimized structures were confirmed to be local minima by the absence of imaginary frequencies. Self-consistent field (SCF) iterations were converged to a DIIS error of at most 10^{-8} Hartree, with tighter convergences of 10^{-10} Hartree being achieved in most cases. Solutions to the Hartree–Fock and Kohn–Sham equations were confirmed to be stable with respect to occupied–virtual mixing. All computations were performed using Q-Chem 5.0.[65]

Electron correlation was incorporated into our computational treatments using both wave function and DFT approaches. In the former case, unrestricted Hartree-Fock reference wave functions were correlated using coupled-cluster theory with single, double, and perturbative triple excitations [CCSD(T)].[66] Coupled-cluster

iterations were taken to be converged when the changes in energy passed below 10^{-8} Hartree and those in the magnitude of the T-amplitudes below 10^{-6}. Unrestricted DFT computations were completed using the ωB97X-V exchange-correlation functional, a combinatorially optimized, range-separated hybrid generalized gradient approximation (GGA) developed by Mardirossian and Head-Gordon.[67] This functional is particularly suitable for the present study because it has been shown to outperform other hybrid GGAs in modeling both transition metal and main-group chemistry[8–10,68,69]. A large (99, 590) integration grid was used in the quadrature for the exchange-correlation potential to ensure the quality of the results.

2.1 Dipole Moments

The dipole moment ($\vec{\mu}$) of isolated CO was determined as a function of its bond length to assist in the interpretation of the EDA results. The ωB97X-V/def2-TZVPD dipole moments were evaluated using linear response theory as implemented in the Q-Chem package.[65] This particular density functional was previously shown to predict dipole moments with high fidelity across a wide range of main group chemical systems.[70] In the present work we further validate the CO dipole moment from ωB97X-V against that obtained using CCSD(T). Because analytic gradients of the energy with respect to orbital rotations were not available for this theory, CCSD(T) dipole moments were obtained using a two-point central finite differences approach to approximate

$$\vec{\mu} = \frac{dE}{d\vec{F}}, \tag{1}$$

where E is the CCSD(T) internal energy, and $\vec{F}$ is an external electric field. Field strengths of $\vec{F} = \pm 1 \times 10^{-4}$ a.u. were used in this analysis, following previous work.[70]

2.2 Energy Decomposition Analysis

The adiabatic absolutely localized molecular orbital energy decomposition analysis (ALMO-EDA) of Mao, Horn, and Head-Gordon[38,61] was used to parse bond lengths, binding energies, and harmonic vibrational frequencies of MCO complexes into contributions from permanent electrostatics, orbital polarization, and charge transfer. While those interested in the details of these terms and their computational implementation should consult the relevant references, a brief overview of the physical content of these terms is helpful at present.

The influence of frozen orbital interactions (permanent electrostatics, Pauli repulsion, and dispersion) on the binding of two molecular or atomic fragments is determined by performing a geometry optimization of the overall complex subject to the constraint that the individual fragment orbitals are determined in isolation and not allowed to relax. The potential energy surface (PES) defined by these constraints is referred to as the frozen (FRZ) surface, and the FRZ contribution to the binding energy (ΔE^{FRZ}) is obtained as the difference between the optimal energy on FRZ surface (E^{FRZ}) and the energy of the isolated fragments, *viz.*

$$\Delta E^{\mathrm{FRZ}} = E^{\mathrm{FRZ}} - \sum_A E_A, \tag{2}$$

where E_A is the isolated energy of fragment A. Note that this definition means stable complexes will have negative binding energies. FRZ contributions to single-fragment observables like bond lengths and harmonic frequencies are evaluated similarly:

$$\Delta\Omega^{\mathrm{FRZ}} = \Omega^{\mathrm{FRZ}} - \Omega_0. \tag{3}$$

Here, Ω^{FRZ} and Ω_0 are the values of the observable on the FRZ and isolated surfaces, and $\Delta\Omega^{\mathrm{FRZ}}$ is the FRZ contribution to the value of the observable.

The effects of polarization (POL) are incorporated by allowing each individual fragment's orbitals to relax in the presence of the other fragment, although mixing between two orbitals on different fragments is forbidden. This amounts to optimizing the supersystem energy by varying the coefficients of the AO-to-MO matrix subject to the constraint that this matrix is fragment-block-diagonal. The POL contribution to an observable ($\Delta\Omega^{\mathrm{POL}}$) is then obtained as

$$\Delta\Omega^{\mathrm{POL}} = \Omega^{\mathrm{POL}} - \Omega^{\mathrm{FRZ}}, \tag{4}$$

where Ω^{POL} is the value of the observable on the POL surface.

Finally, the effects of charge transfer (CT) are obtained as the difference between the structure and properties obtained on the unconstrained PES and those of the POL surface. The CT contribution to an observable of interest ($\Delta\Omega^{\mathrm{CT}}$) is obtained from Ω^{POL} and the value of the observable for the minimum energy structure on the unconstrained surface (Ω^{FULL}) using

$$\Delta\Omega^{\mathrm{CT}} = \Omega^{\mathrm{FULL}} - \Omega^{\mathrm{POL}}. \tag{5}$$

In the complete basis set limit, the distinction between POL and CT becomes blurred, so it is important to consider the effects of basis set superposition error (BSSE) between the fragments. Previous studies using ALMO-EDA have indicated that this effect is minimal up through augmented triple-ζ bases.[38,72] All EDA computations in the present work employ the def2-TZVPD basis, so we assume the BSSE will not be significant on the basis of these previous results.

As defined in the adiabatic EDA scheme, CT is not divided into independent contributions from forward- and back-donation, unlike other EDA schemes. Due to the controversy surrounding the relative importance of these contributions in MCOs, we further analyzed our results by obtaining complementary occupied-virtual pairs (COVPs) of fragment orbitals, following the work of Khaliullin *et al.*[73,74] These computations used the (vertical) ALMO-EDA scheme of Head-Gordon and coworkers,[73–77] which is similar to the adiabatic scheme outlined above, except that the FRZ and POL results are obtained through single point computations using the geometry as optimized on the unconstrained surface. These COVPs represent the most energetically significant CT interactions in the complex. As indicated above, analysis of molecular properties on the basis of the decomposition of energies, as occurs in COVP, is inherently indirect and our analysis of the specific influences of forward- and backward-donation on the

Table 1 Computational and experimental data for MCO complexes of specified multiplicity (M), organized into isoelectronic series. Geometric parameters and harmonic vibrational frequencies were computed using the indicated method with the def2–TZVPD basis set. Unless noted otherwise, binding energies were determined using def2–QZVPD single-point computations on these geometries and include corrections for vibrational zero-point energies. Binding energies are calculated according to Eq. **??**, such that a negative value indicates a stable complex, unlike some other conventions. Harmonic frequency shifts are reported relative to isolated CO, and experimental values were obtained from species in Ne matrices and obtained from values in Ref. 28, unless noted otherwise

Species	M	M−C Length (Å)		C−O Length (Å)		Binding Energy (kcal/mol)		CO Frequency Shift (cm^{-1})		
		CCSD(T)	ωB97X-V	CCSD(T)	ωB97X-V	CCSD(T)	ωB97X-V	CCSD(T)	ωB97X-V	Expt
$TiCO^-$	4	2.020	1.997	1.175	1.175	-80.51	-29.20	-319.2	-388.4	-350.9
VCO	6	1.992	1.996	1.150	1.144	-17.18	-17.58	-169.6	-197.6	-210.2
$CrCO^+$	6	2.169	2.165	1.123	1.117	-60.68	-21.51	77.7	77.0	60.0
VCO^-	5	1.955	1.944	1.172	1.172	-19.20	-19.22	-304.3	-376.7	-334.1
CrCO	7	2.179	2.189	1.137	1.134	-2.31	-2.49	-87.6	-119.4	-122.4
$MnCO^+$	7	2.575	2.556	1.123	1.115	-9.78[a]	-9.68[a]	80.5	97.5	7.2[b]
$CrCO^-$	6	2.155	2.168	1.165	1.171	0.93	-1.70	-461.3	-447.7	-462.8
MnCO	6	2.004	2.008	1.163	1.151	23.87[a]	12.59[a]	-211.1	-195.1	-185.8
$FeCO^+$	4	1.876	1.934	1.130	1.120	-36.08	-33.58	-0.6	45.0	-17.8
$CoCO^-$	3	1.709	1.707	1.195	1.174	-5.49	-17.29	-325.8	-336.0	-320.6
NiCO	1	1.649	1.680	1.157	1.146	-39.52	-30.58	-138.6	-115.3	-134.2
$CuCO^+$	1	1.928	1.923	1.121	1.114	-33.16	-33.17	102.8	114.3	93.6
$NiCO^-$	2	1.718	1.670	1.170	1.169	-27.20	-19.61	-366.5	-260.0	-280.2
CuCO	2	1.910	1.963	1.138	1.134	-6.27	-5.44	-86.9	-124.2	-111.1
$ZnCO^+$	2	2.316	2.330	1.121	1.114	-15.50	-14.90	96.7	113.4	–
$CuCO^-$	3	1.837	1.865	1.181	1.182	11.76	8.71	-377.4	-399.1	-394.6
ZnCO	3	1.955	1.947	1.165	1.162	56.34	54.49	-253.8	-261.5	-288.6[c]

[a] Binding energy single points computed using the def2–TZVPD basis set
[b] Frequency obtained from Ar_3MnCO. Matrix-perturbation was estimated to depress this value by $68.6\,cm^{-1}$, suggesting a gas-phase value of $7.2\,cm^{-1}$. See Ref. 33 and discussion in text.
[c] Ref. 71

basis of COVP results should therefore be treated with caution relative to the adiabatic EDA results that probe geometries and frequencies directly.

In our application of the adiabatic EDA framework, we define the MCO complexes as a supersystem of a metal atom/ion and a neutral, singlet CO molecule. A number of relatively low-energy spin states can be realized for many of the metals of present interest. In this study, spin states were determined on the basis of their computed harmonic CO vibrational frequency (ω_{CO}) and its agreement with experimental values. In most cases this also corresponded to the energetic minimum among the set of possible spin states for a given MCO complex. The few exceptions are noted as they are discussed at length below.

3 Results and Discussion

3.1 Validation of Density Functional Theory

In this work we use energy decomposition analysis (EDA) to provide quantitative and qualitative insights into the physical content of vibrational Stark effects in MCO complexes. The FRZ, POL, and CT contributions (defined above) to bonding in these systems are not physically observable, and so they cannot be compared to experimental results. Furthermore, while a variety of EDA schemes have been developed for DFT and partially correlated wave function theories,[78] EDA for highly correlated, more trustworthy wave function methods like coupled-cluster theory has yet to be realized. Hence, the ωB97X-V structures and properties obtained on the FRZ and POL surfaces cannot be directly validated either by comparison to experiment or to higher-level, systematic theories. Instead, we evaluate the performance of the ωB97X-V functional through its treatment of MCO complexes on unconstrained PESs, as this is a necessary condition for the validity of the remaining results from the EDA. Specifically, we compare ωB97X-V binding energies, bond lengths, and harmonic frequency shifts against those obtained using CCSD(T). We further confirm the quality of our DFT treatment through comparison to experimental frequency shifts. Data used in these comparisons can be found in Table 1.

The ωB97X-V predictions for compound geometries exhibit high fidelity to CCSD(T) results we have obtained. For isolated CO, the ωB97X-V/def2-TZVPD equilibrium bond length is 1.126 Å, in good agreement with both our CCSD(T) result (1.133 Å) and the experimental value of 1.128 Å.[79] For MCO complexes, better agreement is obtained in predictions for the C−O bond lengths (r_{C-O}) than those for the M−C bonds (r_{M-C}) in both absolute and relative terms, though the agreement for both parameters is excellent. The mean absolute errors for the ωB97X-V r_{M-C} and r_{C-O} values, relative to those for CCSD(T), are 0.020 ± 0.018 Å and 0.006 ± 0.005 Å, respectively, where uncertainties are standard deviations. These correspond to relative errors of 1 % for M−C bonds and 0.5 % for C−O bonds. Both theories yield linear geometries for most complexes in this study, though CrCO, $CrCO^-$, and CuCO are all predicted to be bent. We discuss MCO bending at length in Section 3.3.3 below; here we simply note that ωB97X-V overbends complexes by 2.6–6.2° relative to CCSD(T)

for the few bent complexes in this study.

Comparisons between the ωB97X-V and CCSD(T) binding energies found in Table 1 were obtained through single-point computations using the def2-QZVPD basis set and include corrections to account for vibrational zero-point energies (VZPE), unless otherwise indicated; additional binding energies with the def2-TZVPD basis and without the VZPE correction can be found in Table S1, provided in the ESI.† For about half of the compounds studied herein, chemical accuracy (agreement within 1 kcal/mol) between CCSD(T) and ωB97X-V was achieved, while for $CrCO^-$, $FeCO^+$, $CuCO^-$, and ZnCO discrepancies of about 1–4 kcal/mol were obtained. In certain cases the disagreement is egregious: the isoelectronic $CrCO^+$ and $TiCO^-$ systems exhibit errors of 40 and 50 kcal/mol, respectively, with ωB97X-V underbinding the complexes relative to CCSD(T). Absent experimental values for these binding energies, we cannot say with certainty which (if either) value is likely to be correct, although the ωB97X-V energies are closer to the absolute values obtained for the isoelectronic VCO complex, as well as most other MCOs in this study. The errors for the remaining compounds—MnCO, $CoCO^-$, NiCO, and $NiCO^-$—range from 9–12 kcal/mol. Where they exist, discrepancies between energies obtained with these two theories are not systematic: depending on the identity of the metal atom, ωB97X-V may either overbind or underbind the MCO complex relative to CCSD(T).

Shifts in the ω_{CO} upon complex formation ($\Delta\omega_{CO}$), evaluated using ωB97X-V and CCSD(T), are also compared to experimental CO frequency shifts in Table 1. Our frequency anaylsis yields normal modes that, in general, depend on the coordinates of all three atoms in the MCO complex. By ω_{CO}, then, we mean the frequency of the high-energy vibrational mode, which consists almost entirely of a stretching of the C−O bond, even if M moves slightly as well; we will not worry about this distinction in the remainder of the manuscript. Computed vibrational frequencies were not corrected for anharmonicity in the CO bond, rendering comparison of absolute frequencies to experimental results inappropriate. Instead, we compare shifts in the CO frequency upon binding to metal atoms under the assumption that anharmonic effects in free and bound CO are similar. Experimental shifts were determined as

$$\Delta\upsilon_{CO} = \upsilon_{CO}^{bound} - \upsilon_{CO}^{free} \quad (6)$$

using a value of $\upsilon_{CO}^{free} = 2140.8\,cm^{-1}$ obtained in a Ne matrix by Liang and Andrews.[80] Unless noted otherwise in Table 1, values of υ_{CO}^{bound} for MCO complexes were obtained from experiments performed in Ne matrices. Experimentally, these matrices depress υ_{CO} in metal carbonyls by 5–15 cm^{-1}.[28] This perturbation is relatively small, and we expect these absolute matrix effects to approximately cancel in determining $\Delta\upsilon_{CO}$ through Eq. **??**. Small errors in this approximation should not affect our results significantly, since we are concerned with overarching trends in MCOs.

Without including corrections for anharmonicity or matrix effects, ωB97X-V values of ω_{CO} have a mean absolute error of $21.4 \pm 14.7\,cm^{-1}$ with respect to experimental shifts, marginally better than the $24.0 \pm 20.1\,cm^{-1}$ discrepancy between CCSD(T) and experiment. The CCSD(T) and ωB97X-V frequency shifts agree with each other within $31.2 \pm 27.1\,cm^{-1}$. These results are visualized in Figure 2. There is a slight tendency for our computed frequencies to blue-shift relative to experiment, exhibited by mean signed errors of 6.1 and 8.9 cm^{-1} in the ωB97X-V and CCSD(T) frequency shifts, respectively. *Prima facie*, the most egregious errors between our computations and experiment are for $MnCO^+$ and $FeCO^+$, and these are discussed at length in Section 3.3 below.

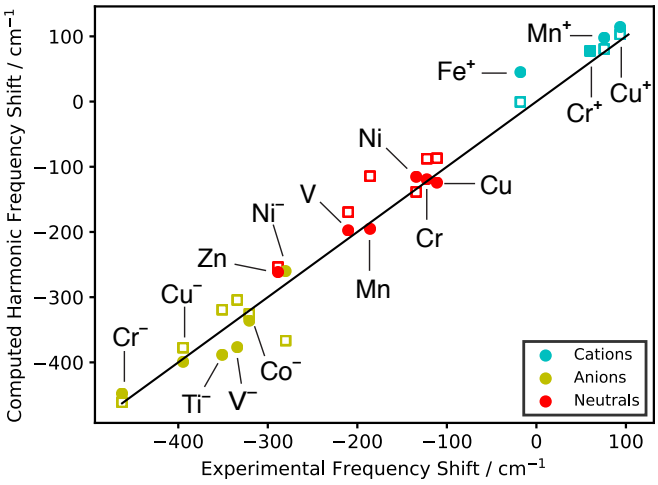

Fig. 2 Comparison of experimental and computational CO frequency shifts in MCO complexes of different charge. ωB97X-V (solid circles) performs well against CCSD(T) (open squares) and experimental frequency shifts (solid line) for species of different charge. Computations performed using the def2-TZVPD basis set. The experimental value for $MnCO^+$ has been corrected for matrix effects following Ref. 33.

While CCSD(T) is the *bona fide* gold standard for modeling the electronic structure of single reference systems, it is known to break down in systems that exhibit significant multireference character and/or strong correlation.[5,81,82] Results from at least one study suggest that transition metal carbonyls are well-treated with single reference methods,[81] lending credence to our computational methodologies. Still, the potential for these difficulties means that we are not completely guaranteed of the trustworthiness of our DFT results, even in the systems where excellent agreement with CCSD(T) was obtained. For the same reason, however, discrepancies between ωB97X-V and CCSD(T) need not necessarily be taken as a failure of the density functional. Indeed, due to the well-known difficulties in determining the electronic structure of transition metals, any individual computation on these systems should be treated with caution, even when state-of-the-art methods are used. The bulk of our analysis of MCO compounds does not pivot on any single result but is derived from a number of results for similar species. We submit, therefore, that the overall agreement between our computational methods and available experimental results lends credence to our DFT treatment on the whole, even if any individual result may be erroneous. Hence, we proceed with optimistic caution in analyzing the bonding in MCO systems using EDA results from the ωB97X-V density functional.

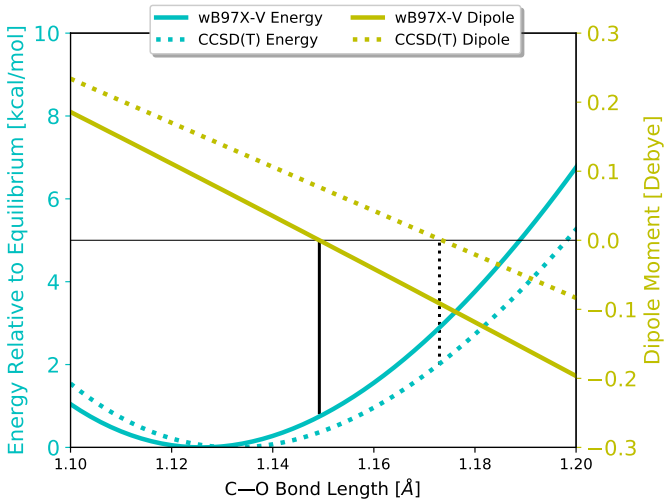

Fig. 3 Binding energy of isolated CO relative to that at the equilibrium bond length, plotted with the absolute dipole moment of CO, both as a function of distance. Results using ωB97X-V/def2-TZVPD (solid) and CCSD(T)/def2-TZVPD (dashed) are compared. The dipole moment vector is oriented from O to C, such that a positive dipole moment corresponds to the localization of negative charge on the carbon atom. Vertical black lines indicate bond lengths where CO exhibits no permanent electric dipole. Energies, dipole moments, and bond lengths are in units of kcal/mol, debye, and angstom, respectively.

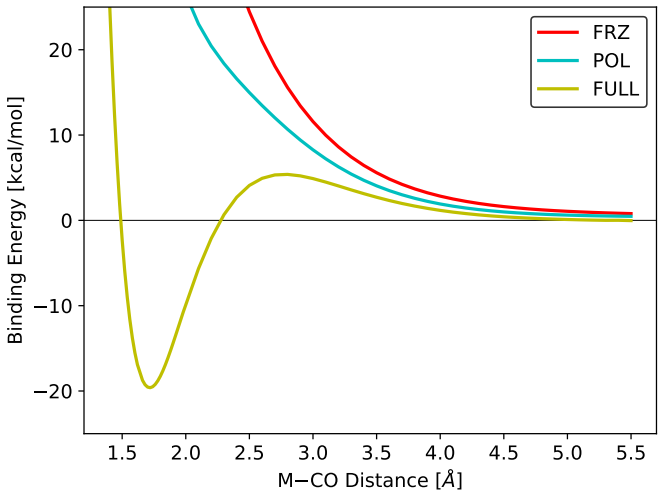

Fig. 4 Frozen, polarized, and unconstrained potential energy surfaces for $CoCO^-$. The energetic zero is defined as the energy of infinitely separated Co^- and CO fragments.

3.2 Bonding in MCO Complexes

After briefly analyzing the computed dipolar properties of free CO, we establish a general model for MCO binding by first considering the most straightforward cationic, anionic, and neutral systems, treating more complicated systems later. Specifically, the "normal" systems are taken to be those where a metal binds CO in a linear fashion on a PES containing the asymptote of its electronic ground state. The remaining systems, which either exhibit a non-linear geometry or bind CO through an excited electronic state on the metal, are incorporated into our general model of MCO binding in Section 3.3 below.

3.2.1 Isolated Carbon Monoxide

Modeling isolated CO is a straightforward but necessary precursor to analyzing physical and chemical features of MCO binding. The equilibrium electric dipole moment ($\vec{\mu}_e$) of CO is particularly important for analyzing the interactions between the M and CO fragments on the FRZ and POL surfaces. At equilibrium, ωB97X-V predicts a CO dipole moment of 0.0884 D oriented toward the O atom (with negative charge on C), in qualitative agreement with the experimental value of $\vec{\mu}_e = 0.1222\,\text{D}$.[83]. Our CCSD(T)/def2-TZVPD prediction of 0.1288 D enjoys even closer agreement with experiment. The discrepancy between CCSD(T) and ωB97X-V predictions of μ_e is not surprising as theoretical treatments of the CO dipole moment are known to depend sensitively on the amount of electron correlation and the size of the basis set that is employed in the computation.[84]

The dipolar properties of CO near its equilibrium bond length are particularly interesting. On the ωB97X-V PES, the CO dipole moment decreases as the bond is stretched, and a dipole-free structure is obtained with $r_{C-O} = 1.149\,\text{Å}$ (Figure 3). This dipole-free structure is destabilized by less than 1 kcal/mol relative to the energetic minimum. As the CO bond continues to stretch beyond 1.149 Å, the dipole moment increases in magnitude, but with a sign opposite that at equilibrium. Similarly, low-energy compressions of CO from its equilibrium structure increase μ_e. While CCSD(T) predictions of near-equilibrium dipole moments, also shown in Figure 3, give a zero-dipole structure with a slightly higher relative energy of 2 kcal/mol, and a markedly higher zero-dipole bond length of 1.173 Å, the qualitative features of stretching and compression are the same. These trends confirm earlier studies of the CO electric dipole moment function determined from experimental vibrational frequencies,[85] and are consistent with the moderately large electric polarizability that has been computed for CO.[86]

Thus, computation and experiment provide a similar picture of CO: stretching and compressing the C−O bond on small length scales causes only minor increases in the electronic energy of the system, accompanied by noticeable changes in μ_e. Intriguingly, small, low-energy perturbations to the C−O bond length can change the magnitude—indeed, the sign—of the molecular dipole moment. These features of the electronic structure of CO provide critical insight into the bonding of MCO systems.

3.2.2 Anionic Complexes (M = Ti^-, V^-, Cr^-, Co^-, Ni^-, Cu^-)

Relative to neutral and cationic species, theoretical treatments of MCO anions are relatively sparse in the literature. In decompositions of both ΔE_{bind} and $\Delta\omega_{\text{CO}}$, binding in various MCO^- systems is along the lines of the DCD model, and so this subset of systems forms a natural starting point for our discussion of metal–carbonyl bonding.

Our computational results indicate that the physical components of the FRZ term (electrostatics, Pauli repulsion, and dispersion) are insufficient to bind anionic MCOs, indicated by the lack of stable bound structures on the FRZ surface. In order to confirm the repulsion between the M^- and CO fragments, we computed rigid-CO dissociation curves for these systems. We present

Table 2 Geometric parameters for selected transition metal monocarbonyls of multiplicity M on different adiabatic EDA surfaces. Values obtained using the ωB97X-V density functional with the def2–TZVPD basis set; this theory predicts the bond length of isolated CO to be 1.126 Å. Missing entries indicate a lack of a bound structure on a given surface.

Species	M	M−C Length (Å)			C−O Length (Å)			MCO Angle (Degree)		
		FRZ	POL	FULL	FRZ	POL	FULL	FRZ	POL	FULL
$TiCO^-$	4	–	–	1.997	–	–	1.175	–	–	180.0
VCO	6	5.582	2.698	1.996	1.126	1.122	1.144	168.2	179.9	179.9
$CrCO^+$	6	2.751	2.362	2.165	1.117	1.114	1.117	180.0	180.0	180.0
VCO^-	5	–	–	1.944	–	–	1.144	–	–	180.0
CrCO	7	5.807	5.373	2.189	1.126	1.126	1.134	180.0	152.0	152.7
$MnCO^+$	7	3.594	2.704	2.556	1.120	1.116	1.115	179.4	180.0	180.0
$CrCO^-$	6	–	4.959	2.168	–	1.126	1.171	–	85.2	134.1
MnCO	6	–	–	2.008	–	–	1.151	–	–	180.0
$FeCO^+$	4	2.774	2.214	1.934	1.117	1.113	1.120	180.0	179.9	179.8
$CoCO^-$	3	–	–	1.707	–	–	1.174	–	–	179.9
NiCO	1	2.332	1.937	1.680	1.123	1.118	1.146	180.0	179.7	179.9
$CuCO^+$	1	2.390	2.052	1.923	1.114	1.112	1.114	180.0	180.0	180.0
$NiCO^-$	2	–	–	1.670	–	–	1.169	–	–	179.9
CuCO	2	4.535	4.427	1.963	1.26	1.126	1.134	144.7	130.5	145.7
$ZnCO^+$	2	3.297	2.398	2.330	1.119	1.114	1.114	180.0	180.0	180.0
$CuCO^-$	3	–	4.562	1.865	–	1.127	1.182	–	99.6	180.0
ZnCO	3	3.287	2.456	1.946	1.124	1.120	1.162	180.0	180.0	180.0

the FRZ surface for $CoCO^-$, displayed as the red curve in Figure 4, as an example of this; additional FRZ surfaces may be found in Figure S1.† These results indicate that the $(M^-)-CO$ interaction is everywhere repulsive on the FRZ surface. Pauli forces are exclusively destabilizing, and dispersion and electrostatics are insufficient to bind anionic MCOs. Even when the C−O bond is stretched enough to reverse the sign of its dipole moment, a repulsive surface is obtained as discussed in the ESI (Figure S2).†

When we include POL effects, the picture of MCO^- binding is largely the same. Most of the POL surfaces do not possess local minima, the exceptions being $CrCO^-$ and $CuCO^-$, which form weakly bound van der Waals (vdW) complexes. As both of these systems exhibit exceptional behavior in other respects as well, a full discussion of their binding is deferred to Section 3.3 below. Despite the formation of vdW complexes in two of the six systems, short range interactions between metal anions and CO are energetically unfavorable on POL surfaces, exemplified by that for $CoCO^-$ in Figure 4 and the remaining systems in Figure S1.† Rationalization of this behavior follows that provided in the preceding paragraph: the effects of intramolecular orbital relaxation are unable to overcome the energetic penalties of Pauli repulsion.

This leaves on explanation for the formation of anionic MCO complexes: charge transfer. As illustrated for $CoCO^-$ in Figure 4 and the remaining anionic systems through the data in Tables 2 and 3, short-range, bound complexes are observed on the unconstrained PESs for all of the MCO^- species considered herein. In the "normal" cases of $TiCO^-$, VCO^-, $CoCO^-$, and $NiCO^-$, we compute sizable binding energies of −22–32 kcal/mol. The computed binding energies of $CrCO^-$ and $CuCO^-$ are small by comparison; indeed, $CuCO^-$ is predicted to be metastable with respect to infinitely separated, ground state Cu^- and CO fragments. Again, discussion of these anomalies is found in Section 3.3 below. The importance of CT in MCO anions is further highlighted by the shape of the unconstrained PES in Figure 4. As the Co^- and CO fragments approach each other from infinite separation, the interaction is repulsive until $r_{Co-CO} \lesssim 2.3$ Å. This initial repulsion is a feature of most of the other anions in this study as well (see discussion in the ESI†). Despite differences in binding energies and PES morphologies, the six anionic MCO complexes of this study are unified by large red shifts in ω_{CO} upon binding. We compute these to be on the order of 300–500 cm^{-1}, in agreement with experimental results (Table 3) as discussed above.

The coupled occupied-valence pair (COVP) analysis[73,75] provides a first-order estimate to the contributions of forward- and back-donation to the overall energy stabilization due to charge transfer. COVP analysis may also provide insight into the sources of shifts in ω_{CO}, but we advise caution here for the reasons described above. Results from this procedure, presented in Figure 5, indicate that the back-donation from the metal anions into unoccupied CO orbitals is the predominant mode of charge transfer for the MCO^- systems we considered, as many have argued previously.[28] Chemical interpretation of this result is routine: negative charge renders the metal anion reluctant to accept additional electron density from CO while enhancing the extent of back donation. Stated differently, the M−CO bond in these systems can be considered a dative covalent bond.

While our results show CT is necessary to bind the MCO anions, the physical interactions included in the FRZ and POL terms are obviously present in the physical systems. In particular, we expect electrostatic and polarization effects to help stabilize the final complexes, as previous EDA results have indicated.[27] But the lack of binding on the FRZ and POL surfaces indicates that electrostatics, dispersion, and polarization do not play a fundamental role in anionic MCO complexes. As such, these systems serve as paradigmatic examples of the DCD model of metal-ligand binding, where electron donation between the ligands dominates

Table 3 Adiabatic energy decomposition analysis of binding energies (kcal/mol) for metal monocarbonyls of a specified spin multiplicity (M). FRZ, POL, and CT values are incremental, as defined in Section 2.2 of the text, and computations were performed using the ωB97X-V density functional with the def2–TZVPD basis set. Positive binding energies indicate that a complex is metastable with respect to ground state fragments, and missing entries a lack of a bound structure at a given level of theory

Species	M	δ(FRZ)	δ(POL)	δ(CT)	δ(Total)
$TiCO^-$	4	–	–	-32.05	-32.05
VCO	6	-0.03	-0.36	-18.88	-19.27
$CrCO^+$	6	-5.27	-11.76	-6.24	-23.27
VCO^-	5	–	–	-22.51	-22.51
CrCO	7	-0.04	-0.01	-3.15	-3.20
$MnCO^+$	7	-2.24	-6.19	-2.84	-11.27
$CrCO^-$	6	–	-0.91	-1.85	-2.76
MnCO	6	–	–	–	10.8
$FeCO^+$	4	-4.88	-17.57	-13.49	-35.94
$CoCO^-$	3	–	–	-22.20	-22.20
NiCO	1	33.96	-30.41	-37.09	-33.54
$CuCO^+$	1	-8.27	-20.01	-6.97	-35.25
$NiCO^-$	2	–	–	-25.02	-25.02
CuCO	2	-0.07	-0.02	-6.19	-6.28
$ZnCO^+$	2	-2.95	-9.77	-4.18	-16.90
$CuCO^-$	3	–	40.39	-34.14	6.25
ZnCO	3	87.44	-3.07	-31.44	52.93

Table 4 Adiabatic energy decomposition analysis of harmonic vibrational frequencies (cm^{-1}) for metal monocarbonyls of a specified spin multiplicity (M). FRZ, POL, and CT values are incremental, as defined in Section 2.2 of the text, and computations were performed using the ωB97X-V density functional with the def2–TZVPD basis set. Missing entries a lack of a bound structure at a given level of theory

Species	M	δ(FRZ)	δ(POL)	δ(CT)	δ(Total)	Expt.
$TiCO^-$	4	–	–	-388.4	-388.4	-350.9
VCO	6	-0.8	40.3	-237.0	-197.5	-210.2
$CrCO^+$	6	86.9	25.0	-34.9	77.0	60.0
VCO^-	5	–	–	-376.7	-376.7	-334.1
CrCO	7	-0.2	0.0	-119.2	-119.4	-122.4
$MnCO^+$	7	56.0	33.3	8.6	97.9	7.2
$CrCO^-$	6	–	-0.2	-447.6	-447.8	-462.8
MnCO	6	–	–	–	-195.2	-185.8
$FeCO^+$	4	84.5	42.0	-81.5	45.0	-17.8
$CoCO^-$	3	–	–	-336.0	-336.0	-320.6
NiCO	1	31.1	69.6	-216.0	-115.3	-134.2
$CuCO^+$	1	114.6	32.3	-32.6	114.3	93.6
$NiCO^-$	2	–	–	-260.0	-260.0	-280.2
CuCO	2	0.2	-0.3	-124.1	-124.2	-111.1
$ZnCO^+$	2	60.0	50.3	3.0	113.3	–
$CuCO^-$	3	–	-5.6	-393.4	-399.1	-394.6
ZnCO	3	15.6	40.9	-318.0	-261.5	-288.6

both ΔE_{bind} and $\Delta\upsilon_{\text{CO}}$.

3.2.3 Cationic Complexes (M = Cr^+, Mn^+, Fe^+, Cu^+, Zn^+)

In contrast to the anionic MCO complexes, where charge transfer effects are responsible for binding, electrostatics and polarization play more important roles for MCO cations. Indeed, among the salient features of the data in Table 2 is the formation of closely bound complexes on the FRZ surfaces of all of the MCO^+ species in the scope of this study. This is unsurprising given the electrostatic properties of isolated CO (*vide supra*): a permanent charge–dipole interaction stabilizes the cationic complex relative to the isolated fragments. Furthermore, the effects of Pauli repulsion are expected to be diminished in the cationic systems, where metal 3*d*- and/or 4*s*-orbitals are more compact relative to those in the corresponding anions.

Altogether, the physics included on the FRZ surface results in binding energies of −2–8 kcal/mol, up to nearly a quarter of the total binding energies for these species. The binding of MCO cations on the FRZ surface is accompanied by moderate compressions in $r_{\text{C}-\text{O}}$ of 0.006–0.012 Å (Table 2) and blue shifts in ω_{CO} of 55–115 cm^{-1} (Table 4). These results can be rationalized using Figure 3, which demonstrates that compression of CO increases the magnitude of its dipole moment, leading to a stronger electrostatic interaction with the metal cation. This CO compression may also be interpreted as a strengthening of the CO bond with an accompanying increase in ω_{CO}, ranging from 50–115 cm^{-1} in the present systems.

Inclusion of the effects of intraatomic orbital relaxation on the POL surface leads to further compression of the C−O bond and additional blue shifts in ω_{CO}. The effects of POL on the C−O bond are less marked than the effects of FRZ interactions, with additional bond compressions and harmonic frequency shifts of 0.002–0.005 Å and 25–50 cm^{-1}, respectively. These effects can be understood as a continuation of the FRZ surface effects just described, where removing the constraint on orbital relaxation allows for additional flexibility in the geometry of CO. Others have also noted that polarization can effect C−O bond contractions in MCO cations.[24] While the impact of POL on the properties of CO is relatively small, it drives significant changes to the binding energies in MCO^+: indeed, POL makes the dominant contribution to binding in these systems, providing 6–20 kcal/mol of stabilization, about half of the overall binding energies (Table 3). Relaxation of the frozen-orbital constraint also impacts the complex geometries significantly, giving rise to 0.3–0.9 Å decreases in M−C bond lengths (Table 2). Taken together, the significant POL effects in the overall MCO^+ complex and the minimal effects on the properties of CO suggest that the bulk of the fragment polarization occurs on the metal cations, which redistribute their 3*d*-/4*s*-orbitals to allow for a closer approach between the fragments, resulting in greater energetic stabilization.

Charge transfer effects provide an additional 3–7 kcal/mol stabilization to the M−CO bond, a contribution of similar magnitude to that from FRZ interactions in most cases. CT also decreases $r_{\text{M}-\text{C}}$ in cations by a few tenths of an angstrom. In two of the five systems (M = Mn^+ and Zn^+), CT gives rise to incremental blue shifts in ω_{CO}. However, in the remaining three cations (M = Cr^+, Fe^+, and Cu^+), we compute that CT actually leads to 30–80 cm^{-1} incremental *red shifts* in ω_{CO}. While they do not report directly on $\Delta\omega_{\text{CO}}$, the COVP results for cations in Figure 5 indicate that these three systems exhibit greater back-donation than both $MnCO^+$ and $ZnCO^+$, where the CT effect on ω_{CO} is negligible.

Our results for the decomposition of $\Delta\omega_{\text{CO}}$ in cationic MCOs

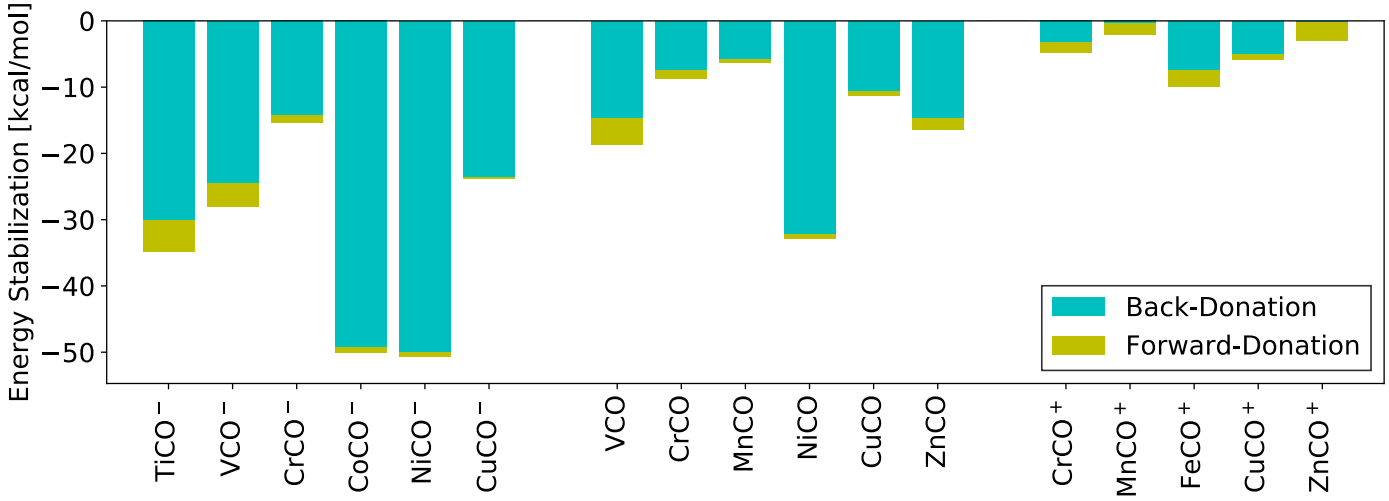

Fig. 5 Coupled occupied-valence pair (COVP) analysis for selected transition metal monocarbonyls. Energy stabilization due to charge transfer is separated into contributions from forward- (CO → M) and back-donation (M → CO).

provide direct contradiction to the standard application of the DCD model for these systems. As noted above, this framework attributes MCO blue shifts to CT, specifically a decreased occupation of the 5σ-orbital on CO. Previous results have already indicated that these blue shifts were not due to CT as argued in the DCD model.[25,40] Our data not only confirm that blue-shifts are due to permanent electrostatics and orbital polarization, but go on to demonstrate that CT effects, where appreciably present, actually *diminish* the amount of blue-shifting observed in non-classical metal carbonyls. While values of $\Delta\omega_{CO}^{CT} = 8.6$ and $3.0\,cm^{-1}$ for $MnCO^+$ and $ZnCO^+$ suggest that some minimal amount of ω_{CO} blue-shifting due to CT may be possible, the magnitude of these shifts is too small to be decisive. Hence, the DCD explanation for ω_{CO} blue shifts is not only incorrect, but qualitatively wrong for most if not all of the relevant cationic MCO systems.

The careful reader will remember that our results for MCO cations exhibited the worst agreement with experiment among our dataset, due to particularly egregious results for $MnCO^+$ and $FeCO^+$. It is therefore sensible to ask again whether we can trust the qualitative trends indicated by our results. It seems that matrix effects account for the discrepancy in $MnCO^+$, though disagreement for $FeCO^+$ persists (see Section 3.3.2 for details). In any case, the results for $FeCO^+$, suggest we *underestimate* the CT red-shifting. For now it is therefore sufficient to note that these results, along with the close agreement for the other cations (Table 1) make it clear that CT does actually promote red-shifting in non-classical metal carbonyls, in contrast to the paradigm of the DCD model.

In summary, a number of overall trends for MCO cations stand out from our dataset. The most notable of these is the significance of FRZ and POL effects in determining $\Delta\omega_{CO}$ and ΔE_{bind}, especially in light of the fact that these are effectively absent in the description of the anionic systems provided above. Polarization plays the dominant role in energetic stabilization of MCO cations. While CT contributions to both the relative and absolute values of ΔE_{bind} and $\Delta\omega_{CO}$ are diminished in cations relative to MCO anions, CT is still an important feature of MCO cations despite previous indications otherwise.[19] A competition between blue-shifts due to FRZ and POL interactions and red-shifts due to CT results in the overall frequencies that are observed experimentally. This is similar to the case of certain hydrogen-bonding systems, where FRZ interactions promote blue-shifting in the C−H bond that is mitigated by the effects of POL and CT.[87] Once these coarse-grained effects are taken into account, the finer details of MCO^+ binding can be understood in light of the occupation of the $4s$-orbital in the metal cation, as discussed in the ESI.†

3.2.4 Neutral Complexes (M = V, Cr, Mn, Ni, Cu, Zn)

The binding motifs of neutral MCO complexes mediate between those of their cationic and anionic counterparts, exhibiting moderate $\Delta\upsilon_{CO}$ red-shifts on the order of 100–300 cm^{-1}. In some ways this reflects the fact that the physical underpinnings of MCO bonds share motifs with both MCO^- and MCO^+ systems. Despite similarities to both of the cases considered previously, the neutral systems present interesting physical phenomena not present in either set of charged systems.

Similar to the cationic systems, bound structures exist on the FRZ surfaces for all of the neutral complexes considered in this study. But where FRZ cations were more tightly bound with binding energies on the order of −2–10 kcal/mol, there is a tendency for neutral metals to form vdW complexes on their FRZ surfaces, indicated by r_{M-C} values of 4.5–5.8 Å and binding energies on the order of hundredths of kcal/mol (Tables 2 and 3, respectively). Absent the permanent electrostatic interactions that govern the FRZ surfaces of charged complexes, neutral MCO complexes are loosely bound by dispersion interactions in their FRZ structures. NiCO and ZnCO are somewhat exceptional, having shorter M−C bonds, though they must still be dispersion-bound as there is no permanent electrostatic contribution and the Pauli term is always repulsive.[76] These two compounds, as well as MnCO, are further interesting in that their metal atoms bind CO through an electronically excited state; this behavior is discussed in Section 3.3.1

below. In the species that form vdW complexes (M = V, Cr, Mn, and Cu), $\Delta\omega_{CO}$ values for FRZ structures are negligible (Table 4). Small blue shifts (15–30 cm^{-1}) are found in NiCO and ZnCO, indicating that the shortening (and strengthening) of the C−O bond increases the strength of dispersion interactions with the metal atom, possibly through charge reorganization in CO.

Polarization effects vary significantly across the neutral species in this study: in some cases, the effects are negligible, while in others they are substantial. The structures, binding energies, and frequency shifts in CrCO, MnCO, and CuCO are largely unperturbed by intramolecular orbital relaxation. In the other three systems (VCO, NiCO, and ZnCO), POL decreases the length of the M−C bond, stabilizes the complexes slightly, and leads to blue shifts in ω_{CO}. The effect on the complex geometry is startlingly large for VCO, where $r^{FRZ}_{V-C} = 5.582$ Å and $r^{POL}_{V-C} = 2.698$ Å—POL leads to a nearly 3 Å contraction in r_{M-C}! Polarization-derived decreases in r_{M-C} for VCO and NiCO are likely due to the unoccupied metal 4*s*-orbital in these systems, which allows a closer approach between the fragments. In the other species, Pauli repulsion between the CO orbitals and the diffuse 4*s*-shell prevents a close approach between the two fragments absent the effects of CT. ZnCO is an exception to this rule because its binding occurs through an excited Zn atom electron configuration (Section 3.3.1). In accordance with the trends seen on the FRZ surfaces, close binding on POL surfaces is accompanied by blue shifts in ω_{CO}. Blue shifts of 40.3, 69.6, and 40.9 cm^{-1} are seen for VCO, NiCO, and ZnCO, respectively.

Relative to the FRZ and POL effects, CT strengthens the binding in neutral MCO complexes significantly, such that all of the neutral metals we studied bind CO covalently in unconstrained computations. Figure 5 indicates that these charge transfer effects are dominated by back-donation, similar to the anionic MCO systems. The charge transfer stabilization in these systems ranges from 3–37 kcal/mol (Table 3) and is roughly correlated with the M−C bond length (Table 2) in the complex. Again ZnCO provides a clear exception to this trend, and this is because Zn binds CO from an electronically excited triplet state, discussed in the following section.

3.3 Anomalous Behavior in MCO Compounds

The preceding results and discussion indicate that the binding motifs in MCO compounds, including the resulting shift in ω_{CO} depends largely on the overall charge, electron configuration, and atomic number of the metal atom. Trends based on these features provide a coherent description of the majority of the compounds in our dataset. Still, a few of the systems under consideration exhibit unique binding modes that warrant further analysis and discussion.

3.3.1 Electronically Excited Metal Atoms: MnCO, NiCO, $CuCO^-$, and ZnCO

The electronic structure in the majority of the MCO complexes of this study can be understood as a perturbation to that of the ground electronic states of the isolated M and CO fragments. In MnCO, NiCO, $CuCO^-$, and ZnCO, however, this is not the case; in these systems the orbitals in the MCO complex are derived from the interaction between CO and an electronically excited metal atom. The concept of bond preparation, commonly employed in cluster models,[88–91] is helpful in the analysis of these systems and is invoked repeatedly below. Simply put, we must first prepare the metal atom/ion for binding through electronic excitation to a state that can interact with the adsorbate, CO in this case, appropriately. For three of these systems, this results in MCO compounds that are only metastable relative to the isolated ground state fragments. In the remaining system, NiCO, the final complex is bound with respect to the ground state fragments, though the electronic structure is particularly complicated due to multiple low-lying electronic configurations.

Table 5 Binding energies and frequency shifts for MCO complexes that form from bond prepared metal atoms, computed at the ωB97X-V/def2-TZVPD level of theory. Electronic binding energies (D_e) with respect to both ground (ΔE^{grd}_{bind}) and bond-prepared (ΔE^{bp}_{bind}) fragments are reported. Experimental CO vibrational frequency shifts ($\Delta\nu^{expt}_{CO}$), reproduced from Table 1, allow unambiguous identification of experimental species. Energies and frequency shifts are in units of kcal/mol and cm^{-1}, respectively.

Species	ΔE^{grd}_{bind}	ΔE^{bp}_{bind}	$\Delta\omega_{CO}$	$\Delta\nu^{expt}_{CO}$
^{6}MnCO	10.8	-25.3	-195.1	-188.8
^{3}NiCO	-10.9	–	-58.0	–
^{1}NiCO	-33.5	-71.5	-115.3	-134.2
$^1CuCO^-$	-1.7	–	-35.2	–
$^3CuCO^-$	6.2	-34.8	-399.1	-394.6
^{1}ZnCO	-0.20	–	0.4	–
^{3}ZnCO	52.9	-35.9	-261.5	-288.6

The isoelectronic Cu^- and Zn atoms bind CO similarly, although differences due to the charge in the resulting complex like those seen above (Section 3.2) persist. Both metals have ground state $[Ar]4s^23d^{10}$ electronic configurations that form dispersion-bound vdW MCO complexes with negligible $\Delta\omega_{CO}$ values according to our ωB97X-V computations (Table 5). These results comport with chemical intuition—stable, fully occupied 4*s* and 3*d* subshells render the metal atoms unlikely to interact with the CO orbitals—but fail to account for the large υ_{CO} red shifts of 394.6 and 288.6 cm^{-1} that have been experimentally observed for $CuCO^-$[92] and ZnCO,[71] respectively. Interestingly, the study that reported the CO stretching frequency for $CuCO^-$ included mixed-basis B3LYP computational results for $^1CuCO^-$ that gave a frequency shift of -331.2 cm^{-1} in qualitative agreement with their experimental result. Subsequent DFT studies[2,31] also determined a singlet ground state for $CuCO^-$. We obtain a similar result of -350.1 cm^{-1} using the B3LYP functional and the def2-TZVPD basis. Yet the inability of both CCSD(T) and ωB97X-V to predict this value for $CuCO^-$ calls the B3LYP results into question.

To investigate alternative binding modes, we obtained CCSD(T) and ωB97X-V results for $^3CuCO^-$ and ^{3}ZnCO. Results from these computations exhibit excellent agreement with the experimental $\Delta\upsilon_{CO}$ results for $CuCO^-$ and ZnCO, suggesting it may be these high-spin species that have been observed experimentally. Indeed, the experimental work that first identified ZnCO

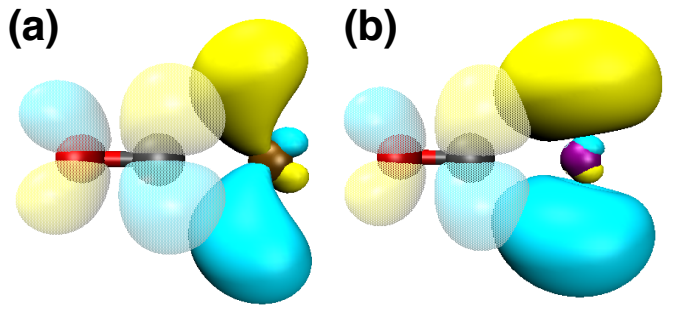

Fig. 6 COVP orbitals for $\pi^* \leftarrow 4p$ back-donation from M to CO for (a) $CuCO^-$ and (b) ZnCO. This is the dominant CT interaction in these systems.

assigned the absorption at 1852.2 cm^{-1} to ^{3}ZnCO on the basis of BP86 calculations.[71] However, as indicated in Table 5, these triplet complexes are destabilized with respect to the ground state fragments by 6.3 and 52.9 kcal/mol, respectively. The metastability of these complexes also explains other aspects of the experimental results. Specifically, the magnitude of the $CuCO^-$ peak was found to decrease relative to those of other species upon matrix annealing,[92] and both $CuCO^-$ and ZnCO peaks disappeared entirely after a period of broadband radiation.[71,92] To the best of our knowledge, the present study provides the first indication that the observed signals for $CuCO^-$ come from the triplet complexes. Furthermore, where previous (singlet) computations led researchers to conclude that $CuCO^-$ exhibited a bent structure,[31,92] the present results predict a linear geometry for this species, as well as ZnCO. Experimentally, our results suggest the Cu^- and Zn atoms undergo electronic excitation to metastable triplet states (bond preparation) during metal vaporization and prior to reaction with CO. Something similar likely occurs in the preparation of alkaline earth metal carbonyls, where excitations into the $(n-1)d$-orbitals facilitate bonding.[37,93]

Working from the conclusion that experimental results for $CuCO^-$ and ZnCO concern triplet states obtained through a bond-prepared $[Ar]4s^14p^13d^{10}$ configuration on the metal, the decomposition of the binding properties for these species follows the general trends for anionic and neutral species as described above. Unlike the other anions in this study, $^3CuCO^-$ forms a vdW complex on its POL surface, although this result is not particularly significant. More interestingly, the extent of CT is significantly enhanced in these two systems. lndeed, $CuCO^-$ and ZnCO exhibit the the largest υ_{CO} red shifts in each of their charge categories (Table 4). The highly diffuse $4p$-orbital exhibits significantly greater spatial and energetic overlap with the CO π^*-orbital than do the more contracted metal $3d$-orbitals (Figure 6). These features allow a much stronger mixing between the donor–acceptor orbitals in the $\pi^* \leftarrow 4p$ interaction, and a significant CT effect ensues. CT energy stabilizations for unconstrained computations on $CuCO^-$ and ZnCO are also among the largest in anions and neutrals, respectively (Table 3), but even so are not significant enough to overcome the initial promotion energy to obtain the triplet metal atoms from the ground state singlets. Previous studies had debated the importance of $4p$-orbitals in metal–carbonyl bonding, finding that $4p$-repolarization can be an important mechanism for diminishing interfragment repulsion, but that CT from $4p$-orbitals was insignificant compared to other CT interactions.[27,47,94] For most cases in the present study, analysis of the COVP orbitals supports the conclusion that $\pi^* \leftarrow 4p$ back-donation is relatively unimportant. But our results for $CuCO^-$ and ZnCO suggest that, at least in some cases, the $4p$-orbitals actually play a defining role in the M−CO bond.

The modes of complex formation for MnCO and NiCO are similar in some ways, though additional complications arise. As in the two cases above, the experimentally observed structures (as determined by the υ_{CO} shift upon complex formation) are formed through the interaction of a ground state CO molecule and an electronically excited, bond-prepared metal atom. For Ni, the ground state $[Ar]4s^13d^9$ configuration excites to $[Ar]4s^03d^{10}$ upon NiCO formation, while for Mn, $[Ar]4s^23d^5$ excites to $[Ar]4s^13d^6$ (Figure 7). In both cases the $4s$-electron excites into the $3d_{z^2}$ orbital, rendering the $4s$-orbital singly occupied such that $4s \leftarrow 5\sigma$ forward-donation becomes possible.[15,52,95] These bond-preparing excitations also significantly diminish the Pauli repulsion in the complex, which is known to be a significant barrier to bond formation in metal carbonyls.[15,22] Hence electronic excitations on Ni and Mn facilitate binding, as in the cases of Cu^- and Zn considered above.

For NiCO, both the ground (^{3}Ni) and excited (^{1}Ni) metal atoms can bind CO, although a more favorable interaction occurs through the excited state. This is in qualitative agreement with the coupled-cluster study of NiCO electronic states by Schaefer, *et al.*.[95] The ωB97X-V functional predicts a bent $^3A'$ NiCO structure for triplet NiCO. While other DFT studies predicted a bent structure similar to our own,[22,30,58] the previously mentioned coupled-cluster study[95] reported the existence of a stable but linear triplet state. Our own CCSD(T) computations confirm/deny the linear structure for ^{3}NiCO. Both our DFT and CCSD(T) treatments predict a linear structure for $^1\Sigma^+$NiCO, the species of present interest in this study.

The PESs for these interactions [Figure 7(a)] suggest that two different modes of binding occur for these structures. In $^1\Sigma^+$NiCO, a vdW complex forms on the FRZ surface as seen for other neutral systems, in contrast to an earlier CSOV result that indicated a repulsive FRZ interaction for ^{1}NiCO.[15] POL and CT further stabilize the M−CO interaction by 30 and 37 kcal/mol increments, respectively (Table 3). This leads to an overall complex binding energy of −33.5 kcal/mol with respect to (ground state) ^{3}Ni and CO (Table 5). $^3A'$ NiCO by contrast, forms vdW complexes on the FRZ and POL surfaces, and a moderately bound ($\Delta E_{bind} = -10.8$ kcal/mol) complex on the FULL surface. We note again that the ωB97X-V structure for $^3A'$ NiCO used in this EDA is bent, in contrast with the CCSD(T) result. Regardless of this discrepancy, the difference in the phenomenology of ^{1}NiCO and ^{3}NiCO binding as predicted by ωB97X-V is likely due to the occupation of the $4s$-orbital in ^{3}Ni, which extends the range of Pauli repulsion, overpowering any dispersion-based attraction between the fragments. Its absence in ^{1}Ni allows the latter effect to dominate, and bound FRZ and POL structures can be obtained.

The $^1\Sigma^+$NiCO surfaces in Figure 7(a) are unusual and deserve

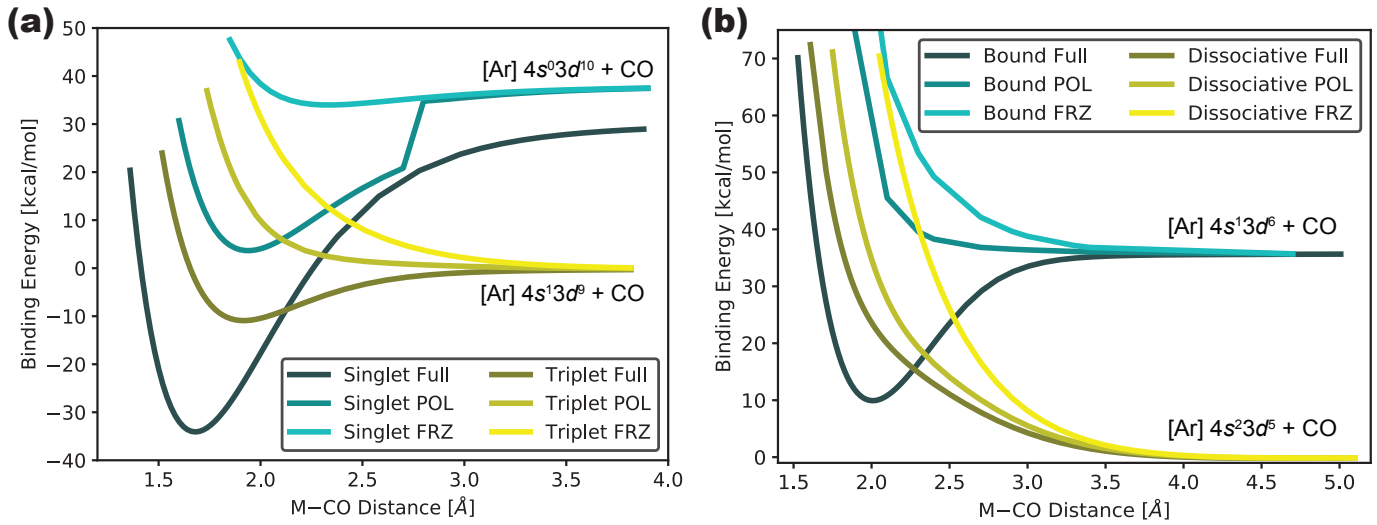

Fig. 7 Potential energy surfaces for the energy decomposition analysis of (a) NiCO and (b) MnCO. In both cases the most tightly bound MCO complex is formed through the interaction of an electronically excited metal atom and ground state CO. See text for discussion of the discontinuity and asymptotes in $^1\Sigma^+$ NiCO dissociation and the absence of FRZ and POL surfaces for bound MnCO.

further comments. In particular, there is an 8 kcal/mol gap between the asymptotes of the full surface and the FRZ/POL surfaces; this is clearly unphysical. Mulliken population analysis reveals charge delocalization errors[96] on the full surfaces that can explain these artifacts. Partial anionic character on Ni spuriously lifts too much degeneracy from the Ni 3*d*-orbitals, giving rise to two distinct asymptotes for the triplet surfaces, as well as the discontinuity in the POL surface, in Figure 7(a). This behavior is discussed more fully in the ESI.†

Delocalization errors notwithstanding, the phenomenology of the $^1\Sigma^+$Ni−CO bond is distinct from that in the other neutral species. Specifically, we find that ^{1}Ni is able to bind CO closely and strongly on both the FRZ and POL surfaces, and furthermore that binding impacts ω_{CO} on these surfaces. This is in marked contrast to the previously discussed neutral species, where FRZ and POL structures were identified as vdW complexes. The compact d^{10}- and empty 4*s*-shells on Ni likely serve to diminish Pauli repulsion and increase the ability of the CO 5σ lone pair to penetrate into the Ni core, stabilizing the Ni−CO bond, as occurs in other systems.[49] Similar effects were seen for V (nominally a $4s^03d^5$ configuration), which binds CO on the POL but not the FRZ surface, but the more compact d^{10}-core in Ni facilitates an ever closer approach between the fragments (Table 2), and thereby a stronger interaction at all stages of the EDA.

Likewise, an excited ^{6}Mn electron configuration leads to the MnCO structure that has been observed experimentally, though in this case both the ground and excited configurations exhibit the same (hextet) spin multiplicity. Computationally, we consider the MnCO binding event to consist first of a bond-preparing excitation from the ground state [Ar] $4s^23d^5$ configuration to an excited [Ar] $4s^13d^6$ state through a $4s \rightarrow 3d_{z^2}$ promotion ($\Delta E =$ 36.1 kcal/mol), followed by interaction with an approaching CO molecule. The bond-prepared binding energy of the resulting complex is −25.3 kcal/mol, leading to an overall destabilization of 10.8 kcal/mol with respect to isolated ground-state Mn and CO. Figure 7(b) presents the ground and excited state potential energy surfaces for MnCO. Unlike in the case for the ground state ^{3}Ni atom, no tightly bound structure was obtained for ground state Mn, although a very weakly bound ($\Delta E_{bind} < 0.2$ kcal/mol) vdW complex was found to be stable on all three surfaces. Analogous to the case for ^{1}NiCO examined in detail above, the electronic difference between these two structures was found to be a result of (lifted) degeneracy among the Mn 3*d*-orbitals.

The excited FRZ and POL surfaces were found to be everywhere dissociative, so the entirety of ΔE_{bind}, geometry changes, and $\Delta\omega_{CO}$ are attributed to CT in Tables 2, 3 and 4. In contrast to the results discussed for $^1\Sigma^+$NiCO in the preceding paragraphs, the nature of the Mn−CO bond is highly similar to that for the other neutral species of this study: FRZ and POL interactions are insufficient to overcome Pauli repulsion, and a bound structure can only be obtained once the effects of CT are included.

Despite subtle differences in the details of these four complexes, the binding motifs of NiCO, MnCO, $CuCO^-$, and ZnCO are unified by the necessity of bond preparation to achieve the ground state complex. In some cases, this insight into the complex formation clears up previous discrepancies between experimental and computational results. Once the metal excitation has been accounted for, the EDA for these systems indicates that MCO binding typically follows the trends determined for the systems of the same charge as presented in Sections 3.2.2 and 3.2.4 above.

3.3.2 Discrepancies with Cations: $MnCO^+$ and $FeCO^+$

The results for $MnCO^+$ and $FeCO^+$ stand out among those for the rest of the species in Table 1 for two reasons: (1) unlike the other cations, experimental results for these systems do not exhibit significant blue shifts in υ_{CO} and (2) the *prima facie* disagreement between theory and experiment is the greatest for these two complexes. This disagreement warrants a closer examination of the

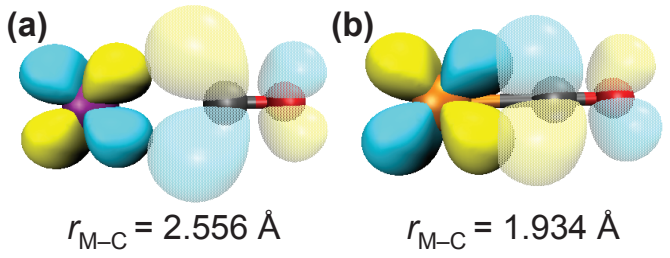

Fig. 8 COVP orbitals for the most significant back-donation interactions in (a) $MnCO^+$ and (b) $FeCO^+$. Metal–carbon bond lengths influence the strength of the interaction and thereby the extent of CT effects on ΔE_{bind} (Table 3) and $\Delta\omega_{CO}$ (Table 4).

experimental results for $MnCO^+$ and $FeCO^+$.

Reed and Duncan report experimental values for $\Delta\upsilon_{CO}$ for $Ar_3(MnCO^+)$ using mass-selected infrared photodissociation spectroscopy.[33] The dissociation spectrum contains two peaks at 2106 cm^{-1} and 2148 cm^{-1}, which they attribute to $Ar_3(^5MnCO^+)$ and $Ar_3(^7MnCO^+)$ on the basis of B3LYP/def2-TZVPP computations. They report additional computational results (at the same level of theory) that indicate that the perturbation due to two Ar atoms red-shifts the CO frequency by 68.6 cm^{-1}. Hence, the experimental result for the $MnCO^+$ frequency shifts in Table 1 should be corrected by 68.6 cm^{-1} in order to remove the effects of the Ar atoms and better facilitate comparison to the computational results. This correction gives value of $\Delta\upsilon_{CO} = 75.8\,cm^{-1}$, in much better agreement with the CCSD(T) and ωB97X-V $\Delta\omega_{CO}$ values of 80.5 and 97.9 cm^{-1}, respectively, as well as the general trend for cations. This also suggests that the anomalously small υ_{CO} blue-shift reported for $MnCO^+$ in Ref. 33 is due to the effects of the Ar atoms present in the experiment, rather than the physics inherent to this MCO complex. Hence, $MnCO^+$ is not as exceptional as it first appears, and the general analysis of Section 3.2.3 carries over to this case.

It is more difficult to reconcile the disagreement between our density functional treatment and the experimental results for $FeCO^+$. Comparison of experimental results for $FeCO^+$ in Ne[97] and Ar[98] matrices indicates that matrix effects are non-trivial for this system: the value of υ_{CO} in solid Ar is red-shifted by 41.5 cm^{-1} relative to that in solid Ne. Hence, we expect the Ne matrix value of 2123.0 cm^{-1} to be noticeably red-shifted from its value in vacuum. This matrix effect may be significant enough to account for the 17.2 cm^{-1} difference between CCSD(T) and experiment, though gas phase determination of υ_{CO} would be necessary to know for sure. It is, however, exceedingly unlikely that this effect can explain the much larger 62.8 cm^{-1} discrepancy for ωB97X-V, the largest in our data set (Table 1).

Furthermore, $\Delta\upsilon_{CO}$ for $FeCO^+$ is lower than we would expect based on the analysis of the other cationic complexes above. According to the results in Table 4, the contributions of FRZ and POL interactions to $\Delta\omega_{CO}$ are similar to those in the other cationic systems considered herein. Instead, $FeCO^+$ stands out because of a relatively large 81.5 cm^{-1} red shift due to charge transfer. We also note that $r_{M-C} = 1.934$ Å in $FeCO^+$ (Table 1), a much shorter bond length than most of the other cations, a result of the low-spin of the complex. This close M−CO approach, and the resulting increase in the overlap of orbitals between the two fragments, facilitates a greater amount of back-donation than in the other cations.[22] Comparison of the COVP orbitals for $MnCO^+$ ($r_{M-C} = 2.556$ Å), where the CT effect is small, and $FeCO^+$ supports this line of reasoning (Figure 8). (Despite a similarly small value for r_{M-C}, a comparable amount of back-donation does not occur for $CuCO^+$ because the additional nuclear charge on Cu^+ diminishes both the spatial and energetic overlap between the metal $3d$- and CO $2\pi^*$-orbitals.) Such an analysis is also supported by the COVP results in Figure 5, which show significant energetic stabilization due to back-donation for $FeCO^+$.

Experimental red-shifting of υ_{CO} for $FeCO^+$[97] obscures the reality that the underlying physics for this system is along the lines of that for the other cations, which all exhibit υ_{CO} blue-shifting. FRZ and POL interactions that increase υ_{CO} compete against the tendency of CT to decrease υ_{CO}. In all cases, including $FeCO^+$, the observed υ_{CO} reports on the overall balance of these interactions.

3.3.3 Bending in MCO Complexes

Finally, we consider metal atoms and ions that form non-linear MCO complexes on their unconstrained PESs. While metal monocarbonyls tend to be linear (see Table 2), exceptions to this rule have been known for some time. Indeed, a number of previous computational studies have indicated that the equilibrium structures of CrCO[22,30,32,58,99–101] and CuCO[22,30,31,58,92,102,103] are non-linear, although at least one wave function (MRCI) study found a linear ground state for CrCO.[?] Two DFT studies of $CrCO^-$ reported predictions that $CrCO^-$ is linear.[2,104] In agreement with the former consensus and in contrast to the latter results, below we report bent ground-state structures for CrCO, $CrCO^-$, and CuCO on the basis of CCSD(T) and ωB97X-V computations (Table 6). (Electronically excited states of these and other MCO compounds have also been found to adopt bent structures,[22,30,100,101] but are not of present interest.) Historically, this MCO bending has been rationalized on the basis that bent geometries diminish the repulsion between the CO 5σ- and metal $3d_{z^2}$- and $4s$-orbitals.[22,58] Our results expand upon this understanding of non-linear MCO complexes.

The geometric data in Table 2 indicate that a variety of mechanisms can promote the linearity of an MCO bond. A linear geometry is obtained for the majority of anionic systems, which are bound almost entirely by CT ($CrCO^-$ is an exception and will be treated below). This suggests that the most favorable orbital overlap is achieved in a linear arrangement, and thus we expect CT to promote linearity in the majority of systems. For the cationic systems, a linear complex is obtained on each of the EDA surfaces. At both the FRZ and POL levels, metal cations bind CO through a favorable charge-dipole interaction (Section 3.2.3) that is maximized when the complex has a linear arrangement. Thus in cations both electrostatic and CT effects promote linear complexes.

The picture is somewhat more complicated in neutral systems, where vdW complexes are found to form on the FRZ and/or POL surfaces in some cases (Section 3.2.4). Most vdW complexes on

Table 6 CCSD(T) and ωB97X-V bond angles (degree) for bent MCO complexes of multiplicity M

Species	M	CCSD(T)	ωB97X-V
CrCO	6	157.9	152.7
$CrCO^-$	7	136.7	134.1
CuCO	2	151.9	145.7

the FRZ/POL surfaces (taken as those with M−C bonds at least 4 Å) are bent. As constraints are removed from the computations, some neutral complexes linearize, while others (CrCO and CuCO) do not. As Fournier observed,[22,58] there is a correlation between the 4*s* occupation of a metal and the linearity of its resulting MCO complex: neutral complexes without a 4*s*-electron tend to be linear, while those with 4*s*-electrons bend, presumably to minimize Pauli repulsion between 4*s*- and 5σ-orbitals. Fournier used this trend to argue that, to the right of V in the transition metal series, low-spin MCO complexes are linear, while high-spin complexes are bent.[22] The linear structure we obtain for ^{1}NiCO, for instance, is an example of this trend. Unlike Fournier, however, we find a bound, linear, and high-spin structure for MnCO, although this structure is only metastable with respect to the ground state fragments (Figure 7). The high-spin ^{3}ZnCO is also linear, presumably to maximize the overlap between the Zn 4*p*- and CO 2π*-orbitals that is critical to binding in this case as shown in Section 3.3.1.

Among neutral complexes, this leaves CrCO and CuCO as our case studies in MCO bending, for which we report ωB97X-V bond angles of 152.7° and 145.7°, respectively (Table 6). Relative to the other complexes in our dataset, each of these compounds is weakly bound ($\Delta E_{\text{bind}} \approx -3$–$6$ kcal/mol [Table 3]). CT is necessary to allow close approach between the two fragments, and even so these three systems have uncharacteristically large M−C bond lengths, on account of repulsion from the 4*s*-electron(s) (Table 2). Analysis of the COVP orbitals in these complexes, presented for CrCO in Figure 9, indicates unique CT interactions for these bent systems. The major forward-donation in these systems occurs through CT from the CO 5σ-orbital into the $3d_{z^2}$- or 4*s*-orbitals for CrCO and CuCO, respectively, similar to the previously considered cases [Figure 9(a)]. The primary back-donation, however, is a $2\pi^* \leftarrow 3d_{z^2}$ interaction [Figure 9(b)], which is forbidden in the linear complex on the grounds of orbital symmetry. This explains how $\Delta\omega_{CO}$ in these two complexes is comparable to similar systems despite longer M−C lengths which would otherwise diminish the extent of CT: three different metal orbitals are able to donate into the CO 2π*-orbital and weaken the bond, unlike in linear complexes.

We finally consider $CrCO^-$, the only bent ion in our series, for which we report an ωB97X-V bond angle of 134.1° (Table 6). At least one previous study reported a linear structure for this system,[104] and to the best of our knowledge the present results are the first indication of a bent structure for $CrCO^-$. Unlike its neutral counterpart and similar to the other anions, $CrCO^-$ does not form a bound structure on the FRZ surface, though a vdW complex forms when POL effects are included. The COVP orbitals for this species are very similar to those depicted for its neutral counterpart in Figure 9, indicating the same, non-standard mode

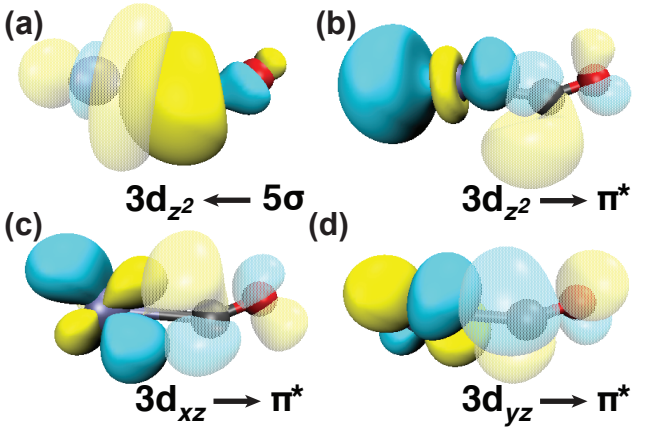

Fig. 9 Most significant COVP orbitals for CrCO: (a) forward-donation and (b)-(d) back-donation. Repulsion between the CO 5σ- and Cr 4*s*-electrons alters the complex geometry and orbital interactions.

of CT discussed above. We therefore motivate the bent structure of $CrCO^-$ as for the neutral species above: bending diminishes σ-repulsion and leads to orbital repolarization to compensate for lost CT stabilization. The destabilizing effects of σ-repulsion are further evident in the fact that $\Delta E_{\text{bind}} = -1.7$ kcal/mol for this complex, much smaller than that for other MCO anions.

It is interesting to compare the structure of $CrCO^-$ to the isoelectronic species MnCO and to $CuCO^-$, which also exhibits a doubly occupied 4*s*-orbital. Both of these complexes are found to be linear in this study on the basis of CCSD(T) and ωB97X-V computations. All previous literature reports of $CuCO^-$ reported a bent structure;[31,92] some computations on MnCO indicated this species was bent[22], and others that it was linear.[30] Bending in MCO complexes occurs to diminish σ-repulsion between the fragments, but comes at the energetic cost of diminishing the overlap of the standard $2\pi^* \leftarrow 3_{d_\pi}$ back-donation that stabilizes these complexes. MCO bending is then the result of two competing interactions between the fragment orbitals. In MnCO it seems sensible to us that linearity is achieved through diminished σ-repulsion vis-à-vis the isoelectronic $CrCO^-$. By contrast, the linearity of $CuCO^-$ almost certainly results from the unique $2\pi^* \leftarrow 4p$ donation that stabilizes this system. The energetic contribution of this interaction, maximized in the linear geometry, prevents bending despite what we assume to be a significant amount of σ-repulsion on the basis of the bent structure for CuCO that we already discussed above. Mutual comparison of CrCO, MnCO, and $CuCO^-$ indicates that the interplay between the interactions that either promote or prevent bending can be quite subtle.

Following Fournier,[22] we understand MCO bending to result from a complicated interplay between minimizing orbital repulsion and maximizing CT stabilization. For Cr and Cu, the singly-occupied 4*s*-orbital and the half- and fully-occupied 3*d*-shells, respectively, repel the CO 5σ-electrons sufficiently to promote bending. We also report the first bent structure for $CrCO^-$, predicted by both CCSD(T) and ωB97X-V, and rationalize this result along the same lines as has been done for neutral systems that are bent. The juxtaposition of these examples against the linear monocarbonyls of Mn and Cu^- elucidates that changes in either the extent

of σ-repulsion or the nature of the CT interactions can dramatically alter MCO complex geometries.

4 Conclusions

Despite the various exceptional cases considered above, a unified picture of MCO binding on the basis of metal charge and orbital occupation emerges from our dataset. The most significant barrier to M−CO bond formation comes from Pauli repulsion due to interactions between the CO 5σ-electrons and metal valence electrons. Various mechanisms can be employed to overcome this repulsion, and the nature of these interactions bears on various experimental observables, like ΔE_{bind} and $\Delta\upsilon_{\text{CO}}$. System charge determines the interplay between these interactions in predictable ways:

- In anions, permanent electrostatics and Pauli repulsion both inhibit binding, and the latter effect is enhanced by diffuse valence orbitals on the metal. These interactions prevent binding absent the inclusion of charge effects, specifically CO ← M back-donation. This leads to large values for ΔE_{bind} in most cases and red-shifted values for υ_{CO} in all of them.

- In cations, permanent electrostatic interactions overcome the destabilizing effects of Pauli repulsion, and orbital polarization facilitates the strengthening of the electrostatic interactions and decreases Pauli repulsion. These effects coincide with C−O bond compression and result in υ_{CO} blue-shifting, which is mitigated by the effects of charge transfer. Polarization of metal valence orbitals contributes about half of ΔE_{bind} for cations.

- Neutral systems exhibit more complicated binding motifs than either ionic system. Charge transfer is the major driving force behind ΔE_{bind}, and compounds are only weakly bound in its absence. Overall υ_{CO} red-shifting is due to charge transfer, though these effects are attenuated by orbital polarization in select cases.

While the significance of charge transfer varies across systems, its effects can hardly ever be neglected in theoretical treatments of MCOs. As has been suggested elsewhere,[32] the lion's share of charge transfer effects on ΔE_{bind} in these systems seems to result from back-donation. Still, we reiterate that caution should be exercised in using parsings of ΔE_{bind} as a proxy for direct analysis of $\Delta\omega_{\text{CO}}$. To a first approximation, this understanding of charge transfer confirms the DCD model, which accounts for M−CO binding through synergistic forward- and back-donation. However, charge transfer almost always promotes υ_{CO} red-shifting, even in systems where overall blue-shifts are observed. This conclusion, informed by previous results,[25,40] directly contradicts the DCD model's picture of υ_{CO} blue-shifts. The DCD model is particularly inapplicable to MCO cations, where permanent electrostatics and orbital polarization play dominant roles.

In select systems, fragment repulsion is overcome by more complicated binding motifs, such as (1) electronic excitations on the metal atom (M = Mn, Ni, Cu^-, Zn) and (2) complex bending (M = Cr, Cr^-, Cu). These features arise through a complicated interplay of orbital interactions, rendering prediction of electronic excitations or complex geometries unlikely.

While we have focused our efforts on understanding the binding of molecular MCOs, the interaction of CO with an extended metal surface is of considerable interest in the broader scientific community. The triatomic MCO system is obviously a crude model for the surface–CO interaction as it neglects the presence of the metal band structure, which can perturb all of the interactions analyzed herein. We can begin to understand the exact nature of this perturbation with reference to cluster models, which help bridge the gap between MCOs and extended systems. These models suggest that σ-repulsion and metal-to-CO π-donation play the dominant role in the surface–CO bond,[105–108] although σ-donation can also be important in some systems.[107] Additionally, as the size of the cluster increases, CO polarization and CT effects vary little with cluster size, while changes to the nature of electrostatic effects and metal orbital polarization can impact binding energies significantly.[106,107] In effect, the metal cluster is more polarizable than an individual atom, enabling more efficient reduction of σ-repulsion.[107] These cluster results suggest that POL may play a much more significant role in extended systems than it does in our present analysis of MCOs, while the nature of CT may remain less changed.

Finally, we note the performance of the ωB97X-V density functional on systems containing first-row transition metals. Results from this functional compare favorably to CCSD(T) predictions of MCO geometries and binding energies in most cases, as well as both experimental and CCSD(T) CO frequency shifts. In cases like $CuCO^-$ and $CrCO^-$, ωB97X-V and CCSD(T) predict qualitatively different geometries and spin states than other DFT treatments, indicating the importance of high-level computations. These results are promising and broadly in line with benchmarks for this functional on other transition metal and main group chemical systems.[9,10,68] Of course, caution should be exercised in using ωB97X-V and other density functionals to study systems with transition metal atoms, particularly when the case of interest is known or expected to exhibit multireference character. But the present study indicates that state-of-the-art density functionals like ωB97X-V can provide valuable insight into the binding of transition metal systems.

Conflicts of interest

There are no conflicts to declare.

Acknowledgements

This material is based upon work supported by the U.S. Department of Energy, Office of Science, Office of Advanced Scientific Computing Research and Office of Basic Energy Sciences, Scientific Discovery through Advanced Computing (SciDAC) program. ER was supported by the University of California through a Chancellor's Fellowship. ER thanks Diptarka Hait for helpful conversations and Yuezhi Mao for access to locally modified versions of the Q-Chem package used to compute EDA surfaces with excited fragments.

Notes and references

1 F. A. Cotton and G. Wilkinson, *Advanced Inorganic Chemistry*, John Wiley & Sons, Inc., New York, New York, 5th edn, 1988, pp. 58–62.

2 G. L. Gutsev, L. Andrews and C. W. Bauschlicher, *Chem. Phys.*, 2003, **290**, 47–58.

3 K. J. P. Schouten, Y. Kwon, C. J. M. van der Ham, Z. Qin and M. T. M. Koper, *Chem. Sci.*, 2011, **2**, 1902–1909.

4 L. G. M. Pettersson, *Top. Catal.*, 2014, **57**, 2–13.

5 D. Rinaldo, L. Tian, J. N. Harvey and R. A. Friesner, *J. Chem. Phys.*, 2008, **129**, 164108.

6 C. J. Cramer and D. G. Truhlar, *Phys. Chem. Chem. Phys.*, 2009, **11**, 10757–10816.

7 M. Sparta and F. Neese, *Chem. Soc. Rev.*, 2014, **43**, 5032–5041.

8 M. Steinmetz, A. Hansen, S. Ehrlich, T. Risthaus and S. Grimme, in *Accurate Thermochemistry for Large Molecules with Modern Density Functionals*, ed. E. R. Jonhson, Springer International Publishing, Cham, 2015, pp. 1–23.

9 S. Dohm, A. Hansen, M. Steinmetz, S. Grimme and M. P. Checinski, *J. Chem. Theory Comput.*, 2018, **14**, 2596–2608.

10 B. Chan, P. M. W. Gill and M. Kimura, *J. Chem. Theory Comput.*, 2019, **15**, 3610–3622.

11 M. J. S. Dewar, *Bull. Soc. Chim. Fr.*, 1951, **18**, C71–C79.

12 J. Chatt and L. A. Duncanson, *J. Chem. Soc.*, 1953, 2939–2947.

13 I. H. Hillier and V. R. Saunders, *J. Chem. Soc. D*, 1971, 642–643.

14 D. E. Sherwood and M. B. Hall, *Inorg. Chem.*, 1980, **19**, 1805–1809.

15 C. W. Bauschlicher, P. S. Bagus, C. J. Nelin and B. O. Roos, *J. Chem. Phys.*, 1986, **85**, 354–364.

16 T. Ziegler, V. Tschinke and C. Ursenbach, *J. Am. Chem. Soc.*, 1987, **109**, 4825–2837.

17 J. Allison, A. Mavridis and J. F. Harrison, *Polyhedron*, 1988, **7**, 1559–1572.

18 L. A. Barnes and C. W. Bauschlicher, *J. Chem. Phys.*, 1989, **91**, 314–330.

19 A. Mavridis, J. F. Harrison and J. Allison, *J. Am. Chem. Soc.*, 1989, **111**, 2482–2487.

20 K. Pierloot, P. Verbeke and L. G. Vanquickenborne, *Inorg. Chem.*, 1988, **28**, 3059–3063.

21 G. Blyholder and M. Lawless, *J. Am. Chem. Soc.*, 1992, **114**, 5828–5832.

22 R. Fournier, *J. Chem. Phys.*, 1993, **99**, 1801–1815.

23 S. Dapprich and G. Frenking, *J. Phys. Chem.*, 1994, **99**, 9352–9362.

24 R. K. Szilagyi and G. Frenking, *Organometallics*, 1997, **16**, 4807–4815.

25 A. J. Lupinetti, S. Fau, G. Frenking and S. H. Strauss, *J. Phys. Chem. A*, 1997, **101**, 9551–9559.

26 G. Frenking and N. Fröhlich, *Chem. Rev.*, 2000, **100**, 717–774.

27 A. Diefenbach, F. M. Bickelhaupt and G. Frenking, *J. Am. Chem. Soc.*, 2000, **122**, 6449–6458.

28 M. Zhou, L. Andrews and C. W. B. Jr., *Chem. Rev.*, 2001, **101**, 1931–1961.

29 C.-F. Huo, Y.-W. Li, G.-S. Wu, M. Beller and H. Jiao, *J. Phys. Chem. A*, 2002, **106**, 12161–12169.

30 J. Pilme, B. Silvi and M. E. Alikhani, *J. Phys. Chem. A*, 2003, **107**, 4506–4514.

31 G. Wu, Y.-W. Li, H.-W. Xiang, Y.-Y. Xu, Y.-H. Sun and H. Jiao, *J. Mol. Struct.: THEOCHEM*, 2003, **637**, 101–107.

32 C. Koukounas, S. Kardahakis and A. Mavridis, *J. Chem. Phys.*, 2005, **123**, 074327.

33 Z. D. Reed and M. A. Duncan, *J. Am. Soc. Mass. Spectrom.*, 2010, **21**, 739–749.

34 A. D. Brathwaite, Z. Reed and M. A. Duncan, *J. Phys. Chem. A*, 2011, **115**, 10461–10469.

35 A. M. Ricks, Z. E. Reed and M. A. Duncan, *J. Mol. Spectrosc.*, 2011, **266**, 63–74.

36 W. Xu, X. Jin, M. Chen, P. Pyykkö, M. Zhou and J. Li, *Chem. Sci.*, 2012, **3**, 1548–1554.

37 X. Wu, L. Zhao, D. Jiang, I. Fernández, R. Berger, M. Zhou and G. Frenking, *Angew. Chem. Int. Ed.*, 2018, **57**, 3974–3980.

38 Y. Mao, Q. Ge, P. R. Horn and M. Head-Gordon, *J. Chem. Theory Comput.*, 2018, **14**, 2401–2417.

39 I. H. Hillier and V. R. Saunders, *Mol. Phys.*, 1971, **22**, 1025–1034.

40 A. S. Goldman and K. Krogh-Jespersen, *J. Am. Chem. Soc.*, 1996, **118**, 12159–12166.

41 J. B. Johnson and W. G. Klemperer, *J. Am. Chem. Soc.*, 1977, **99**, 7132–7137.

42 R. F. Frey and E. R. Davidson, *J. Chem. Phys.*, 1989, **90**, 5541–5554.

43 P. S. Bagus, K. Hermann and C. W. Bauschlicher, *J. Chem. Phys.*, 1984, **81**, 1966–1974.

44 C. W. Bauschlicher, S. R. Langhoff and L. A. Barnes, *Chem. Phys.*, 1989, **129**, 431–437.

45 L. A. Barnes, M. Rosi and C. W. Bauschlicher, *J. Chem. Phys.*, 1990, **93**, 609–624.

46 P. S. Bagus, K. Hermann and C. W. Bauschlicher, *J. Chem. Phys.*, 1984, **80**, 4378–4386.

47 C. W. Bauschlicher and P. S. Bagus, *J. Chem. Phys.*, 1984, **81**, 5889–5898.

48 K. L. Kunze and E. R. Davidson, *J. Phys. Chem.*, 1992, **96**, 2129–2141.

49 E. R. Davidson, K. L. Kunze, F. B. C. Machado and S. J. Chakravorty, *Acc. Chem. Res.*, 1993, **26**, 628–635.

50 K. Morokuma, *J. Chem. Phys.*, 1971, **55**, 1236–1244.

51 K. Morokuma, *Acc. Chem. Res.*, 1977, **10**, 294–300.

52 C. W. Bauschlicher, *J. Chem. Phys.*, 1986, **84**, 260–267.

53 A. Veldkamp and G. Frenking, *Organometallics*, 1993, **12**, 4613–4622.

54 G. Blyholder, *J. Phys. Chem.*, 1964, **68**, 2772–2777.

55 G. Blyholder and M. C. Allen, *J. Am. Chem. Soc.*, 1969, **91**,

3158–3162.
56 A. Nilsson and L. G. M. Pettersson, in *Chemical Bonding on Metal Surfaces*, ed. R. Rioux, Springer New York, New York, NY, 2010, pp. 253–274.
57 K. M. Gameel, I. M. Sharafeldin and N. K. Allam, *Phys. Chem. Chem. Phys.*, 2019, **21**, 11476–11487.
58 R. Fournier, *J. Chem. Phys.*, 1993, **98**, 8041–8050.
59 B. Tremblay and L. Manceron, *Inorg. Chem.*, 2008, **47**, 4531–4535.
60 P. S. Bagus and G. Pacchioni, *J. Phys. Conf. Ser*, 2008, **117**, 012003.
61 Y. Mao, P. R. Horn and M. Head-Gordon, *Phys. Chem. Chem. Phys.*, 2017, **19**, 5944–5958.
62 F. Weigend and R. Ahlrichs, *Phys. Chem. Chem. Phys.*, 2005, **7**, 3297–3305.
63 D. Rappoport and F. Furche, *J. Chem. Phys.*, 2010, **133**, 134105.
64 F. Weigend, F. Furche and R. Ahlrichs, *J. Chem. Phys.*, 2003, **119**, 12753–12762.
65 Y. Shao, Z. Gan, E. Epifanovsky, A. T. Gilbert, M. Wormit, J. Kussmann, A. W. Lange, A. Behn, J. Deng, X. Feng, D. Ghosh, M. Goldey, P. R. Horn, L. D. Jacobson, I. Kaliman, R. Z. Khaliullin, T. KuÅŻ, A. Landau, J. Liu, E. I. Proynov, Y. M. Rhee, R. M. Richard, M. A. Rohrdanz, R. P. Steele, E. J. Sundstrom, H. L. W. III, P. M. Zimmerman, D. Zuev, B. Albrecht, E. Alguire, B. Austin, G. J. O. Beran, Y. A. Bernard, E. Berquist, K. Brandhorst, K. B. Bravaya, S. T. Brown, D. Casanova, C.-M. Chang, Y. Chen, S. H. Chien, K. D. Closser, D. L. Crittenden, M. Diedenhofen, R. A. D. Jr., H. Do, A. D. Dutoi, R. G. Edgar, S. Fatehi, L. Fusti-Molnar, A. Ghysels, A. Golubeva-Zadorozhnaya, J. Gomes, M. W. Hanson-Heine, P. H. Harbach, A. W. Hauser, E. G. Hohenstein, Z. C. Holden, T.-C. Jagau, H. Ji, B. Kaduk, K. Khistyaev, J. Kim, J. Kim, R. A. King, P. Klunzinger, D. Kosenkov, T. Kowalczyk, C. M. Krauter, K. U. Lao, A. D. Laurent, K. V. Lawler, S. V. Levchenko, C. Y. Lin, F. Liu, E. Livshits, R. C. Lochan, A. Luenser, P. Manohar, S. F. Manzer, S.-P. Mao, N. Mardirossian, A. V. Marenich, S. A. Maurer, N. J. Mayhall, E. Neuscamman, C. M. Oana, R. Olivares-Amaya, D. P. OâĂŹNeill, J. A. Parkhill, T. M. Perrine, R. Peverati, A. Prociuk, D. R. Rehn, E. Rosta, N. J. Russ, S. M. Sharada, S. Sharma, D. W. Small, A. Sodt, T. Stein, D. StÃijck, Y.-C. Su, A. J. Thom, T. Tsuchimochi, V. Vanovschi, L. Vogt, O. Vydrov, T. Wang, M. A. Watson, J. Wenzel, A. White, C. F. Williams, J. Yang, S. Yeganeh, S. R. Yost, Z.-Q. You, I. Y. Zhang, X. Zhang, Y. Zhao, B. R. Brooks, G. K. Chan, D. M. Chipman, C. J. Cramer, W. A. G. III, M. S. Gordon, W. J. Hehre, A. Klamt, H. F. S. III, M. W. Schmidt, C. D. Sherrill, D. G. Truhlar, A. Warshel, X. Xu, A. Aspuru-Guzik, R. Baer, A. T. Bell, N. A. Besley, J.-D. Chai, A. Dreuw, B. D. Dunietz, T. R. Furlani, S. R. Gwaltney, C.-P. Hsu, Y. Jung, J. Kong, D. S. Lambrecht, W. Liang, C. Ochsenfeld, V. A. Rassolov, L. V. Slipchenko, J. E. Subotnik, T. V. Voorhis, J. M. Herbert, A. I. Krylov, P. M. Gill and M. Head-Gordon, *Mol. Phys.*, 2015, **113**, 184–215.
66 K. Raghavachari, G. W. Trucks, J. A. Pople and M. Head-Gordon, *Chem. Phys. Lett.*, 1989, **157**, 479–483.
67 N. Mardirossian and M. Head-Gordon, *Phys. Chem. Chem. Phys.*, 2014, **16**, 9904–9924.
68 L. Goerigk, A. Hansen, C. Bauer, S. Ehrlich, A. Najibi and S. Grimme, *Phys. Chem. Chem. Phys.*, 2017, **19**, 32184–32215.
69 D. Hait and M. Head-Gordon, *Phys. Chem. Chem. Phys.*, 2018, **20**, 19800–19810.
70 D. Hait and M. Head-Gordon, *J. Chem. Theory Comput.*, 2018, **14**, 1969–1981.
71 L. Jiang, Y.-L. Teng and Q. Xu, *J. Phys. Chem. A*, 2006, **110**, 7092–7096.
72 P. R. Horn and M. Head-Gordon, *J. Chem. Phys.*, 2015, **143**, 114111.
73 R. Z. Khaliullin, A. T. Bell and M. Head-Gordon, *J. Chem. Phys.*, 2008, **128**, 184112.
74 R. Z. Khaliullin, A. T. Bell and M. Head-Gordon, *Chem. Eur. J.*, 2009, **15**, 851–855.
75 R. Z. Khaliullin, E. A. Cobar, R. C. Lochan, A. T. Bell and M. Head-Gordon, *J. Phys. Chem. A*, 2007, **111**, 8753–8765.
76 P. R. Horn, Y. Mao and M. Head-Gordon, *Phys. Chem. Chem. Phys.*, 2016, **18**, 23067–23079.
77 P. R. Horn, Y. Mao and M. Head-Gordon, *J. Chem. Phys.*, 2016, **144**, 114107.
78 J. Thirman and M. Head-Gordon, *J. Chem. Phys.*, 2015, **143**, 084124.
79 O. R. Gilliam, C. M. Johnson and W. Gordy, *Phys. Rev.*, 1950, **78**, 140–147.
80 B. Liang and L. Andrews, *J. Phys. Chem. A*, 2000, **104**, 9156–9164.
81 W. Jiang, N. J. DeYonker and A. K. Wilson, *J. Chem. Theory Comput.*, 2012, **8**, 3171–3179.
82 I. W. Bulik, T. M. Henderson and G. E. Scuseria, *J. Chem. Theory Comput.*, 2015, **11**, 3171–3179.
83 J. S. Muenter, *J. Mol. Spec.*, 1975, **55**, 490–491.
84 G. E. Scuseria, M. D. Miller, F. Jensen and J. Geertsen, *J. Chem. Phys.*, 1991, **94**, 6660–6663.
85 C. Chackerian, R. Farrenq, G. Guelachvili, C. Roseetti and W. Urban, *Can. J. Phys.*, 1984, **62**, 1579–1585.
86 O. Christiansen, C. Hätig and J. Gauss, *J. Chem. Phys.*, 1998, **109**, 4745–4757.
87 Y. Mao and M. Head-Gordon, *Chem. Phys. Lett.*, 2019, **10**, 3899–3905.
88 I. Panas, J. Schüle, P. Siegbahn and U. Wahlgren, *Chem. Phys. Lett.*, 1988, **149**, 265–272.
89 P. E. M. Siegbahn, L. G. M. Pettersson and U. Wahlgren, *J. Chem. Phys.*, 1991, **94**, 4024–4030.
90 P. Siegbahn, M. Nygren and U. Wahlgren, *Cluster Models for Surface and Bulk Phenomena*, Plenum Press, New York, 1992, pp. 267–279.
91 L. Triguero, U. Wahlgren, P. Boussard and P. Siegbahn, *Chem. Phys. Lett.*, 1995, **237**, 550–559.
92 M. Zhou and L. Andrews, *J. Chem. Phys.*, 1999, **111**, 4548–4557.

93 X. Wu, L. Zhao, J. Jin, S. Pan, W. Li, X. Jin, G. Wang, M. Zhou and G. Frenking, *Science*, 2018, **361**, 912–916.
94 D. Spangler, J. J. Wendolosky, M. Dupuis, M. N. L. Chen and H. F. S. III, *J. Am. Chem. Soc.*, 1981, **103**, 3985–3990.
95 L. Horný, A. Paul, Y. Yamaguchi and H. F. Schaefer, *J. Chem. Phys.*, 2004, **121**, 1412–1418.
96 A. J. Cohen, P. Mori-Sánchez and W. Yang, *Chem. Rev.*, 2012, **112**, 289–320.
97 M. Zhou and L. Andrews, *J. Chem. Phys.*, 1999, **110**, 10370–10379.
98 M. Zhou, G. V. Chertihin and L. Andrews, *J. Chem. Phys.*, 1998, **109**, 10893–10904.
99 J. Kim, Y. S. Lee and H. Ihee, *Int. J. Quantum Chem.*, 2007, **107**, 458–463.
100 J. Kim, T. K. Kim, J. Kim, Y. S. Lee and H. Ihee, *J. Phys. Chem. A*, 2007, **111**, 4697–4710.
101 V. I. Bolshakov, V. V. Rossikhin, E. O. Voronkov, S. I. Okovytyy and J. Leszczynski, *J. of Comput. Chem.*, 2007, **28**, 778–782.
102 C. W. Bauschlicher, *J. Chem. Phys.*, 1994, **100**, 1215–1218.
103 L. Jiang and Q. Xu, *J. Phys. Chem. A*, 2007, **111**, 2690–2696.
104 L. Andres, M. Zhou, G. L. Gutsev and X. Wang, *J. Phys. Chem. A*, 2003, **107**, 561–569.
105 P. S. Bagus, C. J. Nelin and C. W. Bauschlicher, *Phys. Rev. B*, 1983, **28**, 5423–5438.
106 K. Hermann, P. S. Bagus and C. J. Nelin, *Phys. Rev. B*, 1987, **35**, 9467–9473.
107 G. Pacchioni and P. S. Bagus, *J. Chem. Phys.*, 1990, **93**, 1209–1214.
108 P. S. Bagus and G. Pacchioni, *Surface Science*, 1992, **278**, 427–436.